Long-term deep intracerebral microelectrode recordings in patients with drug-resistant epilepsy: Proposed guidelines based on 10-year experience

Katia Lehongre, Virginie Lambrecq, Stephen Whitmarsh, Valerio Frazzini, Louis Cousyn, Daniel Soleil, Sara Fernandez-Vidal, Bertrand Mathon, Marion Houot, Jean-Didier Lemaréchal, et al.

NeuroImage 254 (2022) 119116

Contents lists available at ScienceDirect

NeuroImage

journal homepage: www.elsevier.com/locate/neuroimage

Long-term deep intracerebral microelectrode recordings in patients with drug-resistant epilepsy: Proposed guidelines based on 10-year experience

Katia Lehongre[a,1], Virginie Lambrecq[a,b,c,1], Stephen Whitmarsh[a], Valerio Frazzini[a,b,c], Louis Cousyn[a,c], Daniel Soleil[d], Sara Fernandez-Vidal[a], Bertrand Mathon[a,e], Marion Houot[f,g,h], Jean-Didier Lemaréchal[a,i], Stéphane Clemenceau[e,2], Dominique Hasboun[a,j], Claude Adam[c], Vincent Navarro[a,b,c,k,*]

[a] Sorbonne Université, Paris Brain Institute – Institut du Cerveau, ICM, INSERM, CNRS, APHP, Pitié-Salpêtrière Hospital, Paris France
[b] AP-HP, EEG Unit, Neurophysiology Department, Pitié-Salpêtrière Hospital, DMU Neurosciences, Paris, France
[c] AP-HP, Epilepsy Unit, Pitié-Salpêtrière Hospital, DMU Neurosciences, Paris, France
[d] Bureau d'Etudes CEMS, 801 Route d'Eyguieres, 13 560 Senas, France
[e] AP-HP, Neurosurgery Department, Pitié-Salpêtrière Hospital, Paris, France
[f] Centre of Excellence of Neurodegenerative Disease (CoEN), AP-HP, Pitié-Salpêtrière Hospital, Paris, France
[g] Institute of Memory and Alzheimer's Disease (IM2A), Department of Neurology, AP-HP, Pitié-Salpêtrière Hospital, Paris, France.
[h] Clinical Investigation Centre, Institut du Cerveau et de la Moelle épinière (ICM), Pitié-Salpêtrière Hospital Paris, France
[i] Institut de Neurosciences des Systèmes, Aix-Marseille Université, Marseille, France
[j] AP-HP, Neuroradiologiy Department, Pitié-Salpêtrière Hospital, Paris, France
[k] AP-HP, Center of Reference for Rare Epilepsies, Pitié-Salpêtrière Hospital, Paris, France

ARTICLE INFO

Keywords:
Drug-resistant epilepsy
sEEG
Human
Microelectrode
Multi-unit activity
Technical guidelines

ABSTRACT

Purpose: Human neuronal activity, recorded *in vivo* from microelectrodes, may offer valuable insights into physiological mechanisms underlying human cognition and pathophysiological mechanisms of brain diseases, in particular epilepsy. Continuous and long-term recordings are necessary to monitor non predictable pathological and physiological activities like seizures or sleep. Because of their high impedance, microelectrodes are more sensitive to noise than macroelectrodes. Low noise levels are crucial to detect action potentials from background noise, and to further isolate single neuron activities. Therefore, long-term recordings of multi-unit activity remains a challenge. We shared here our experience with microelectrode recordings and our efforts to reduce noise levels in order to improve signal quality. We also provided detailed technical guidelines for the connection, recording, imaging and signal analysis of microelectrode recordings.

Results: During the last 10 years, we implanted 122 bundles of Behnke-Fried hybrid macro-microelectrodes, in 56 patients with pharmacoresistant focal epilepsy. Microbundles were implanted in the temporal lobe (74%), as well as frontal (15%), parietal (6%) and occipital (5%) lobes. Low noise levels depended on our technical setup. The noise reduction was mainly obtained after electrical insulation of the patient's recording room and the use of a reinforced microelectrode model, reaching median root mean square values of 5.8 μV. Seventy percent of the bundles could record multi-units activities (MUA), on around 3 out of 8 wires per bundle and for an average of 12 days. Seizures were recorded by microelectrodes in 91% of patients, when recorded continuously, and MUA were recorded during seizures for 75 % of the patients after the insulation of the room. Technical guidelines are proposed for (i) electrode tails manipulation and protection during surgical bandage and connection to both clinical and research amplifiers, (ii) electrical insulation of the patient's recording room and shielding, (iii) data acquisition and storage, and (iv) single-units activities analysis.

* Corresponding author at: AP-HP, Epilepsy Unit, Pitié-Salpêtrière Hospital, 47-83 Boulevard de l'Hôpital, Paris 75013, France.
E-mail address: vincent.navarro@aphp.fr (V. Navarro).

[1] These authors contributed equally to this work.

[2] In Memoriam: Dr. Stéphane Clemenceau (1960 - 2021) was a great neurosurgeon, who has spent his entire career in the Department of Neurosurgery at The Pitié-Salpêtrière Hospital (Paris). He founded the epilepsy surgery unit in 1990 and developed advanced techniques for epilepsy surgery, particularly for mesial temporal lobe resections. He was one of the first neurosurgeons to use MRI-guidance instead of angiography for intracranial EEG electrode implantations.

https://doi.org/10.1016/j.neuroimage.2022.119116.
Received 26 August 2021; Received in revised form 23 February 2022; Accepted 15 March 2022
Available online 19 March 2022.

Conclusions: We progressively improved our recording setup and are now able to record (i) microelectrode signals with low noise level up to 3 weeks duration, and (ii) MUA from an increased number of wires . We built a step by step procedure from electrode trajectory planning to recordings. All these delicate steps are essential for continuous long-term recording of units in order to advance in our understanding of both the pathophysiology of ictogenesis and the neuronal coding of cognitive and physiological functions.

1. Introduction

Intracranial electroencephalography (iEEG) investigation prior to epilepsy surgery represents a rare opportunity to access human neuronal assemblies function *in vivo* for extended periods of time. A surgical implantation of intracerebral electrodes can delineate the epileptogenic focus, called the seizure onset zone (SOZ), when non-invasive electroencephalography (EEG) and neuroimaging have been insufficient to localize the epileptogenic focus in drug-resistant patients (Crandall et al., 1963; Engel et al., 2005; Reif et al., 2016; Zijlmans et al., 2019).

Different types of electrodes can be surgically implanted, alone or in combination: subdural strip electrodes, grid electrodes, or depth electrodes for stereoelectroencephalography (sEEG). All of these electrodes contain several *macrocontacts*, spaced several millimeters to centimeters apart. Each macrocontact has a size of a few mm and measures neuronal activity from a large population of neurons (Buzsáki et al., 2012; Parvizi and Kastner, 2018).

Microelectrodes have small contact areas at the tip of isolated wires, with a diameter of around 40 µm. Compared to macrocontacts, *microwires* provide two main advantages: an increased spatial resolution, allowing the recording of local field potentials (LFPs) at submillimeter scale from small neuronal assemblies; and the ability to record action potentials of sampled neurons, i.e.multi-unit activities (MUAs) from which single-unit activities (SUAs) can be isolated after spike sorting (Pedreira et al., 2012; Stacey et al., 2013). The first acute recordings of units in the human mesial temporal lobe were made in 1971, during and between seizures (Verzeano et al., 1971). Macroelectrodes have been modified to allow the insertion of a flexible bundle of microwires (Babb et al., 1973). Subsequently, *microelectrodes* have been inserted for the duration of the iEEG in the epileptogenic focus in humans (Babb and Crandall, 1976; Wyler et al., 1982) and different microelectrode types have been developed. Hybrid depth electrodes have microcontacts interspaced between macrocontacts (Howard et al., 1996). In the Ad-Tech Behnke-Fried macro-microelectrodes model (Fried et al., 1997), microwires are inserted through the macroelectrode shaft, protruding into the cerebral tissue beyond the tip of the depth macroelectrode. In the DIXI hybrid macro-microelectrodes model, the microwires exit the macroelectrode shaft between macrocontacts and have a tetrode rather than a single-wire configuration (Despouy et al., 2019). The Utah array is a two dimensional array of 4 mm × 4 mm that contains 96 microelectrodes and can be implanted at the surface of the cortex (Schevon et al., 2008). Lastly, high density poly(3,4-ethylenedioxythiophene) polystyrene sulfonate (PEDOT:PSS) microelectrodes were recently proposed, for acute recordings in the operative room during surgery (Paulk et al., 2021).

Microelectrodes are implanted in patients with epilepsy for research purposes and the analysis of the LFP, MUA or SUA recorded have provided valuable insights into neuronal codes or underlying physiological processes, as well as cognition (Axelrod et al., 2019; Ekstrom et al., 2003; Fried et al., 1997; Kim et al., 2019; Kreiman et al., 2000; Lakretz et al., 2021; Mormann et al., 2008; Quiroga et al., 2005). Recordings allow testing of cognitive processes such as working and episodic memory, with temporal precision through single-trial studies in brain areas without epileptic activities. For example, important findings were obtained in the mesial temporal lobe, in the amygdala and hippocampus with Behnke-Fried electrodes (Fried et al., 1997), where the isolation of SUA was essential to describe individual neurons' behaviors. Itzak Fried's group described category specific SUA, such as imagery neurons in the human mesial temporal lobe (Kreiman et al., 2000) and place cells in the human hippocampus (Ekstrom et al., 2003). Some mesial temporal lobe SUAs could be selectively activated by distinct pictures of given objects, landmarks or individuals, such as "Jennifer Aniston neuron" (Quiroga et al., 2005). Long-term recordings (up to 3 weeks) during presurgical implantation allow dedicated time periods for cognitive tasks, which can be repeated over several days and weeks. This has obvious value for studying memory encoding and retrieval (Kornblith et al., 2017; Rutishauser et al., 2021; Staresina et al., 2019).

Microelectrode recordings have also been a major tool for investigating the pathophysiology of epilepsy, notably the ictogenesis, i.e. how the brain initiates seizures. Epileptic seizures on EEG are the main electrophysiological marker of epilepsy. Recognizing the most precocious and faster components of the ictal discharge is a key step in identifying the SOZ (Fisher et al., 1992; Talairach and Bancaud, 1966; Wendling et al., 2003). Microelectrodes inserted in the SOZ can capture single-unit activities at the beginning and the development of seizures and help to describe SOZ networks (Lambrecq et al., 2017; Schevon et al., 2012, 2008). In addition, according to the waveform and firing properties of isolated neurons through spike sorting, it is possible to distinguish putative pyramidal cells and interneurons, and to describe their respective involvement in the generation of seizures (Elahian et al., 2018; Truccolo et al., 2011; Weiss et al., 2016). Microelectrodes have also been used to describe single unit behaviors during interictal events like epileptic spikes and have shown heterogeneous firing patterns (Alvarado-Rojas et al., 2013; Despouy et al., 2019; Keller et al., 2010; Ulbert et al., 2004). Microelectrodes can also detect other epileptic markers that are not detected on adjacent macroelectrodes, such as high frequency oscillations (HFOs), specifically in the fast ripple band (250-500 Hz). Initially identified from microelectrode recordings, HFOs were assumed to be generated by small neuronal assemblies of about one mm^3 (Zijlmans et al., 2017). Microelectrodes have also revealed microseizures as discrete rhythmic activities that would not be detected by macroelectrodes, due to the better resolution of microelectrodes for sampling the local field potentials of much smaller neuronal assemblies (Schevon et al., 2008; Staba et al., 2014; Stead et al., 2010).

Detection of units on microelectrodes signal requires a high signal to noise ratio (SNR), that depends on the noise level in the signal but also on the distance of the electrode from the soma of the neuron (Rey et al., 2015; Buzsáki et al., 2012). The higher the noise level is, the more difficult it is to detect action potentials of lower amplitude. The accuracy of the spike sorting algorithm to assign the action potentials detected to different neurons will also be affected by a high noise level because of an alteration of the action potential waveforms (Buccino et al., 2020; Chaure et al., 2018; Wild et al., 2012). As for all electrophysiological recordings, electro-magnetic noise from the surrounding environment, as well as movement artifacts are major noise sources for the signal. Therefore, and because it is not possible to move the microwire of the Behnke-Fried electrode to approach the soma of a neuron, it is crucial to decrease those noise sources, especially because microwires have a very small diameter, that makes them very fragile and sensitive to noise (Misra et al., 2014).

Furthermore, epileptic events, in particular seizures, have unpredictable occurrences and require continuous and long-term electrophysiological monitoring to be recorded. Studying LFPs and unit activity during those events is only possible with stable high quality microelectrode recordings during the whole monitoring period. Long-term microelectrode recordings are also essential for physiological and cognitive stud-

ies at the cellular level. However, continuous and long-term recordings with microelectrodes are technically highly challenging. Thanks to a strong collaboration between several clinical teams of Pitié-Salpêtrière Hospital (Paris, France) and a research center (Paris Brain Institute), located on the hospital's site, we started to record epileptic patients with Behnke-Fried microelectrodes in 2010.

The aim of this paper is to share our experience of the last 10-year with continuous long-term microelectrode recordings and bring recommendations complementary to already published methodological papers. Electrode manipulation during the surgery is a crucial step to avoid noise resulting from wire degradation and has been described in several papers (Misra et al., 2014; Minxha et al., 2018). Detailed quantification of noise level depending on technical setting is important as well to adopt the best methodology, but has not been quantified and described in detail from our knowledge. We have described the technical issues we faced, and the different improvements we made to reduce the noise level on the signal, which is crucial to increase the possibilities to record MUA and SUA. We have first described our current recording methodology in the Method section. The improvement of our data quality over time is reported in the Results section with detailed noise level measures and a quantification of multi-units recordings depending on different material setups. In addition, we have summarized the main technical guidelines, from surgery to recordings, that we found essential to improve the quality of microelectrode recordings.

2. Materials and methods

2.1. Patients

Since 2010, fifty-six patients with refractory focal epilepsy underwent a presurgical intracerebral electrode investigation with additional microelectrodes. The aim of the clinical intracerebral investigation was to determine the SOZ when non-invasive explorations were inconclusive. Non-invasive explorations included medical history, neurological examination, brain imaging (e.g. MRI, PET, SPECT) and long-term scalp video-EEG monitoring. The continuous (24/7) video-EEG monitoring with intracranial electrodes took place in the Epilepsy Unit of the Pitié-Salpêtrière Hospital (Paris, France) and started the day after the implantation. Recordings lasted for 2 to 3 weeks, depending on whether enough informative seizures were recorded. All patients provided informed and written consent for the implantation of microelectrodes, which received approval from local ethic committees (CPP Paris VI, CNRS, 2004, 2006; INSERM C11-16, C19-55).

2.2. Planning of stereotactic electrode placement

Electrode planning was carried out by epileptologists, neurosurgeons and neuroradiologists, days or weeks before implantation. Macroelectrode trajectories and targets were defined only based on clinical objectives. They were very specific to each patient and trajectories were not necessarily orthogonal to the brain surface. The planification of macro-microelectrodes trajectories was not influenced by the decision of adding a microelectrode. Microelectrodes were added to a macroelectrode when there was enough gray matter beyond the last macrocontact for the microwires to expand into. As the original 20 mm length of the microwires was too long, they were cut at a length calculated during trajectory planning.

Until end of 2017, macroelectrode trajectories were planned according to a stereotactic Leksell frame and based on pre-implantation brain MRI, using iplan® stereotaxy, version 3.0, BrainLAB System (Budke et al., 2018; Ringel et al., 2009). Since the end of 2017, the ROSA robot (Zimmerbiomet, Ind., USA) has been used to assist the surgery. However, the ROSA planning software did not allow to map 3D cortical surfaces or to visualize multiple electrode trajectories simultaneously. Therefore, the STIM core facility of the Paris Brain Institute developed a stereotactic sEEG toolbox (EPILOC). One of its modules, STEREO-PLAN (Fernandez-Vidal et al., 2019), allows clinicians to perform sEEG planning. EPILOC includes several image processing pipelines: corregistation of multimodal pre-operative sequences, anatomical segmentations and computation of patient specific models and a dedicated 3D SLICER (Fedorov et al., 2012) graphic interface. The graphic interface allows to visualize all the previous pipeline results, referenced to the ACPC native orientation, and to easily plan and edit trajectories with different depth electrode models. Multiple structural and metabolic imaging modalities (such as PET and SPECT data) can also be merged in the native patient space, to add further information pertinent to the planning of intracerebral trajectories.

2.3. Surgical placement of the electrodes

The stereotactic implantation of intracranial electrodes was performed in the Department of Neurosurgery. Prior to the insertion of microelectrodes into the dedicated hollow macroelectrodes, microwires were cut by the neurosurgeon to the desired length defined during the planning (generally 2-3 mm, Supp. Fig. 1). They were cut using Yasargil microscissors, all at the same length and perpendicularly to the electrode axis, and then gently bend outwards until they had a splayed pattern, like an "umbrella", that will be maintained when they extend in the brain. (Fig. 1). This splayed pattern provides a better chance of recording action potentials (Babb et al., 1973; Misra et al., 2014). All electrodes were fixed on the skull with hollow screws that prevent post-surgical movement of the electrodes (*anchor bolts*: ADTECH LSBK1-BX-06 length 13mm, and LSBK1-AX-06 length 21mm). Once all intracranial electrodes were implanted, the patient's skin was cleaned and sanitized with soap, water and betadine. The head was then prepared for long-term video-EEG recording with careful bandaging (Fig. 2 and Table 1), necessary to avoid any damage to the electrodes and to improve comfort of the patient during hospitalization.

A post-operative CT-scan and MRI were always performed after implantation and merged with the presurgical MRI to verify the electrodes' positions (see 2.6.2). An X-ray was also performed to confirm the spreading of the microelectrodes.

2.4. Connection to the recording system

Patients were connected to the acquisition system during the first day after implantation. First, all supplemental EEG scalp electrodes were placed on the patient's head (where there were no implanted electrodes). A ground electrode was placed under the collarbone, and 2 ECG electrodes were placed on the chest. Secondly, the depth electrode tails were connected to CABRIO connectors (Ad-Tech ®, Wisconsin) for the macroelectrodes and CHET headstages (Neuralynx®, Inc., Bozeman, MO) for the microelectrodes (Fig. 3, Tables 2 and 3). Connecting the tails is a crucial step in the electrode manipulation and requires a lot of care. We therefore established a procedure to increase the patient's comfort, avoid any wrong manipulation and tensile load on the electrode tails that could break the wires, and avoid any tension on connection cables that could lead to disconnection. To maintain sterility, the bandage done in the surgery room was not removed until the patient was discharged. Steps G to J from Fig. 3 were redone every 2 to 3 days in order to repaste the scalp electrodes, but connectors were not moved to avoid manipulating the electrode tails.

2.5. Recording material

2.5.1. Electrodes

The number of macroelectrodes that were implanted in each patient ranged from 4 to 13, including 1-4 hybrid macro-microelectrodes. All electrodes were produced by Ad-Tech Medical Instrument Corporation (Ad-Tech®, Wisconsin). The standard macroelectrodes consisted of 4-12 platinum contacts of 1 mm of diameter, 2.41 mm of length and 5 mm of inter-contact distance with nickel-chromium wiring and polyurethane

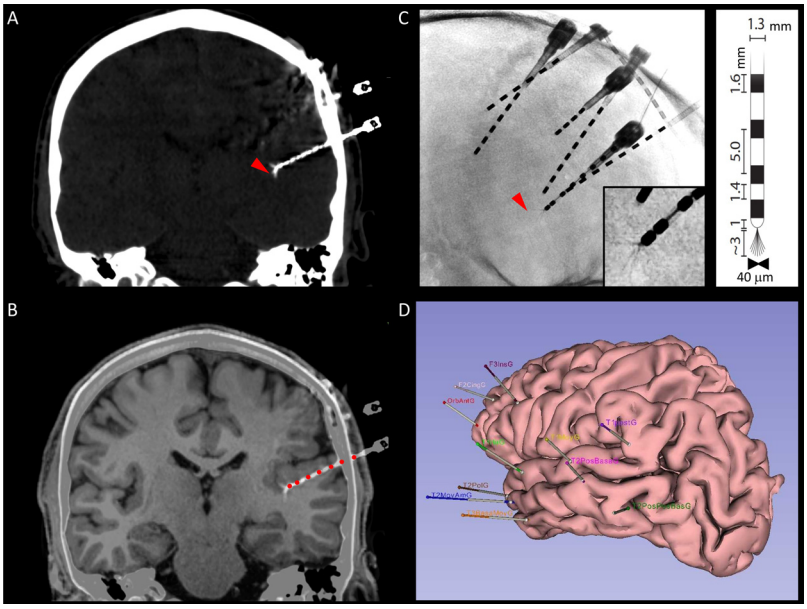

Fig. 1. Multimodal microelectrode identification. A. Cranial CT Scan on a coronal plan showing the trajectory of the macroelectrodes and the localization of microelectrode bundles (red arrow). **B**. Automated superposition of the CT scan with the anatomical T1 MRI, allowing the visualization of microelectrodes' position in the brain parenchyma together with the automated identification of macroelectrode contacts (red circles) along the intracerebral trajectory. **C**. Radiographic image showing the bidimensional location of intracerebral electrodes. The red arrow indicates the location of a microelectrode bundle, seen in the previous pictures. *Inset's*: magnification of microelectrode wires. Note the spreading of the microwires. *Inset's on the right*: Schematic representation of the macro-micro electrode geometry. **D**. 3D Epiloc anatomical reconstruction of subject cortical anatomy, showing the implantation scheme of the intracerebral macroelectrodes.

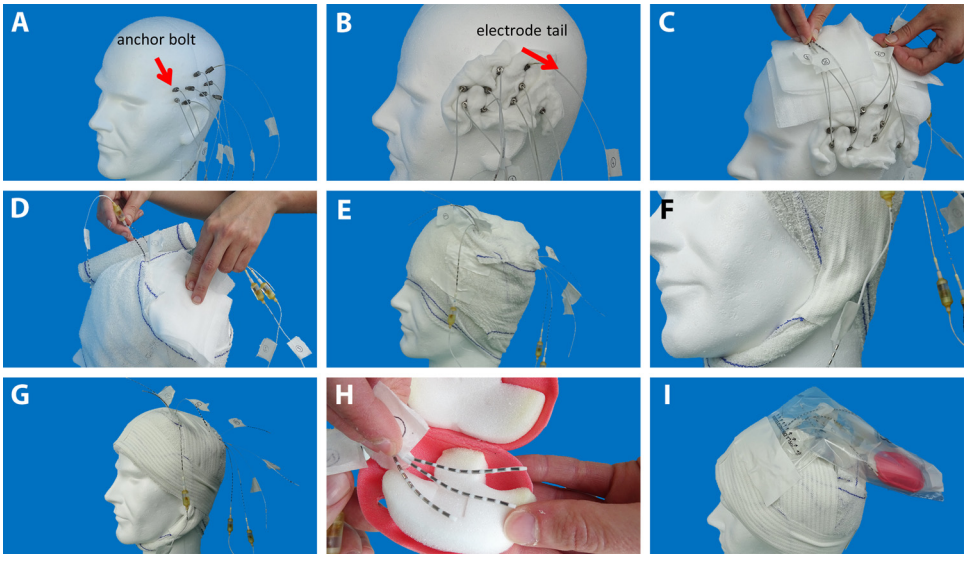

Fig. 2. Main steps for the surgical bandage. A. Surgically implanted macroelectrodes and macro-microelectrodes. The arrow shows an anchor bolt. **B.** Compresses wrapped around the anchor bolts of macro and microelectrodes. The arrow shows an electrode tail. **C.** Bundling of tails in one or two parts above the head. **D.** Fixing together with compresses and bandages while avoiding to cover the electrode tails. **E.** Output of electrode tails through the bandage in 2 different sites. **F.** Making a chin strap. **G.** Coronal and sagittal adhesive strips to hold the bandage in place. **H.** Infusion protection box to protect microelectrodes before connection. **I.** Protection of all connectors and boxes in a plastic bag placed above the head, before connection in the patient's room.

Table 1
Guidelines on electrode tails manipulation and protection during surgical bandage.

	Corresponding pictures from Fig. 2
Wrapping of compresses around the anchor bolts for the patient's comfort (to prevent irritation of the skin around the anchor) and to avoid sharp bending of the electrode tails at the anchor bolt outputs.	A -> B
Grouping of the electrode tails toward the desired output from the bandage. It is important to maximize the output length of the tails from the bandage to avoid any bending or pulling during the connection of the tails to the connectors. If the distance between the electrodes is too long, two outputs from the bandage should be prepared.	C
Covering of the head with bandages without covering the electrode tails and with respect to the prepared output of tails.	D -> G
Protection of microelectrode tails in an infusion box maintained in a plastic bag at the top of the head, to avoid any bad manipulation of tails between the surgery and the connection (i.e. during CT scan / MRI, sleep, etc.).	H + I

tubing. The macro-microelectrodes (Behnke-Fried model) included both a hollow macroelectrode and a microelectrode bundle that spread out from the tip of the macroelectrode. The macroelectrode part of the micro-macroelectrode consisted of 8 (BF08R-SP05X-000, BF08R-SP71X-0C2) or 9 (BF09R-SP05X-0MF, BF09R-SP61X-0BB) platinum contact electrodes of 1.3 mm of diameter and 1.57 mm of length, embedded on the surface of a polyurethane tube with a hollow lumen. The microelectrode, consisted of a bundle of 8 (model 1: WB08R-SP00X-0AA) or 9 (model 2: WB09R-SP00X-0AA; model 3: WB09R-SP00X-014) platinum-iridium microwires of 40 µm diameter and 20 mm length. For all models, the microelectrode bundle was inserted through the hollow macroelectrode, protruding 3-6 mm into the cerebral tissue beyond the tip of the macroelectrode. For model 2 and 3, the 9th wire was un-insulated and was provided for a possible use as reference. The suppression of the insulation on several millimeters confers to this electrode a lower impedance and therefore a capacity to record from a larger neuronal

Fig. 3. Main steps for the electrode connection. A&B. Bandage preparation with holes to add scalp electrodes outside the implanted zone. **C.** Placement of scalp electrodes. **D.** Pasting of velcro bands on the bandage. **E.** Connection and placement of the connectors on the velcro bands. The arrows show the 2 connector types: CABRIO connectors from Ad-Tech and CHETs from Neuralynx. *Note that Neuralynx CHETs are closed with a plastic clip to prevent them from opening. These clips are made of small electrical raceways. Simple tape can be used too, but is less handy and often leaves the CHET sticky when removed.* **F.** Grouping of all the connector cables within a bandage. **G.** Covering of the connectors with compresses. **H.** Covering of the connectors with the "conductive tissue". **I.** Covering and stabilizing with 2 bandages. **J.** Final covering with a net. **K.** Connection to the headboxes. The arrow shows a head box. **L.** Placement of the headboxes in a bag. **M&N.** Fixation of the input and output cables on the bag. The arrows show how the cables are fixed. **O.** The bag is carried by the patient when moving.

Table 2
Guidelines on electrode tails manipulation and protection during connection.

	Corresponding pictures from Fig. 3
Opening of small bandage parts outside the implanted zone, to create access for scalp electrodes	A + B
Placement and pasting of scalp electrodes	C
Preparation of velcro bands that will be used to fix the connectors on the head and prevent any pulling on the electrode tails: •Pasting of velcro bands on the wrap, outside the implanted area but preferentially on the top of the head, where the patient will not lie on while sleeping. •Pasting of small complementary pieces of velcro on all connectors	D
Connection and placement of the connectors on the velcro without pulling and bending of tails and cables. Electrode tails, especially for micros, must be handled very carefully to avoid unnecessary tensile load. The placement will be done: •According to the length of tail available •With all connector cables in the same direction in order to join them on a single side of the patient •With some compresses under tails to avoid bending if necessary	E + F
Wrapping of all connector cables together for the comfort of the patient but also to prevent from pulling on them	F
Covering of tails and connectors with compresses to smooth the compression of the cables with the bandage. Compresses should also be added under the macro-microelectrode tails if needed	G
Covering of the compresses with an electrically conductive silver cloth (Stretch conductive fabric, Less EMF Inc., Latham NY 12110, USA) to shield poorly isolated electrode tails. The tissue is grounded to the patient through an alligator clip attached to the tissue	H
Covering with a bandage and a tubular net bandage to maintain the connectors and the tissue on the patient's head	I + J
Connection of the connector cables to the headboxes and placing of the headboxes in a waist bag that will be carried by the patient if he needs to move. To prevent any disconnection, the connector cables and the output tether cables are attached to the bag. The tether cables are also attached to the amplifier carriage before their connection to the amplifier.	K -> O

Table 3
Glossary.

Name	**Definition**
Electrode tail (Fig. 2B)	Output of the electrode from the brain
CABRIO connector (Fig. 3E)	Ad-Tech electrode connector
CHET (Fig. 3E)	Neuralynx electrode connector
HeadBox (Fig. 3K)	Connection box used to connect electrode connectors and send the signal to the amplifiers
Tether cable	Connection cable from the headboxes to the amplifier

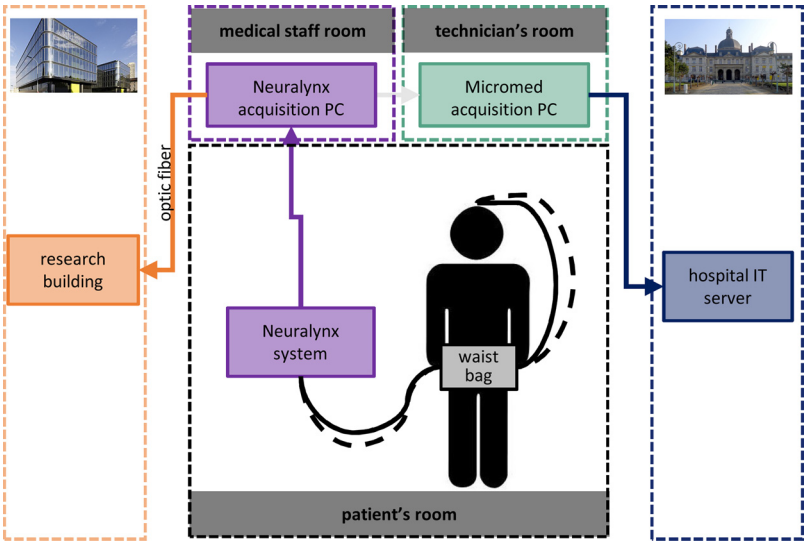

Fig. 4. Current acquisition setup. Signals recorded from macro and microelectrodes are acquired by the research Neuralynx system and sent from the Neuralynx acquisition PC to the clinical Micromed acquisition PC through a direct network connection. The research and clinical acquisition PC send respectively the data to the research and clinical servers to fill the respective databases. The research building is located in the hospital and has a direct network connection to the epilepsy center building via a dedicated optic fiber. Black dashed lines represent cables for macroelectrodes, black plain lines represent cables for microelectrodes.

population, with less sensitivity to action potentials from surrounding neurons (Jurczynski et al., 2021). Model 3 was the same as model 2, but with an epoxy reinforcement on the area of attachment between tails of the microelectrode and macroelectrode (Supp Fig. 1), supposed to reduce the risk of failure at this weak point.

Additional scalp electrodes were also recorded (T9, FT9, Fp1, Fz, Fp2, FT10, T10, O1, Oz, O2, EKG). In the last 23 patients, electrodes essential for polysomnographic recordings (C4 or C3, M1 or M2, E1, E2 and EMG) were added.

2.5.2. Amplifiers

Over the last 10 years, three successive acquisition setups have been used, each one bringing specific improvements (Fig. 4 and Supp. Fig. 2).

Oct. 2010 - Jun. 2012 - Macro and micro recorded on 2 different amplifiers (11 patients): For the first microelectrode recordings, macro and microelectrode signals were acquired on two different amplifiers. All macroelectrode signals were recorded continuously with the clinical amplifier (SD LTM, Micromed® S.p.A., Italy, 128 channels at 1024 Hz), and microelectrode signals were recorded a few hours per day, with the Lynx amplifier (Digital Lynx, Neuralynx®, Inc., Bozeman, MO, 32 channels at 32 kHz, Supp. Fig. 2.A). Macro and micro signals were synchronized offline with the help of an analogical trigger sent to both systems during acquisition.

Nov. 2012 - Oct. 2018 - Macro and micro recorded on same amplifiers (39 patients): In 2012, the Neuralynx system was upgraded to the ATLAS amplifier (Atlas, Neuralynx®, Inc., Bozeman, MO), to record with up to 160 electrodes. Contrary to the previous system, the ATLAS amplifier also allowed the recording from all macro and microelectrodes simultaneously, as well as continuously during the whole clinical investigation of the patient, i.e. up to 3 weeks. Signals from macroelectrodes and microelectrodes were recorded at 4 and 32 kHz, respectively. Because clinicians need access to the data via the clinical database, the signal of the macroelectrodes (and the microelectrodes when the total number of electrodes did not exceed 128) was also recorded by the clinical Micromed systems (1024 Hz). To record the signal in parallel, the signal was split using a specific cable provided by Neuralynx (MDR50), with a Neuralynx connection on one side and touch proof outputs for the Micromed HeadBoxes on the other side (Supp. Fig. 2.B).

Nov. 2018 - current - Macro and micro recorded on a unique amplifier (6 patients): In 2018, the Micromed acquisition software was updated with a network connection between the Neuralynx and Micromed systems, allowing for a real-time data transfer from the Neuralynx acquisition system to the Micromed software and database. Consequently, since 2018 only the ATLAS amplifier has been used to record all electrodes continuously and during the whole clinical investigation (Fig. 4). This new setup avoided a duplication of the electrode connections to two different amplifiers, which was a source of possible connection errors as each electrode was connected twice. Potential noise issues related to the fact that two amplifiers were grounded together, were also avoided. The acquisition sampling rate on Neuralynx was set to 4096 Hz for the macroelectrodes and 32768 Hz for the microelectrodes. Signal from all electrodes was downsampled to 1024 Hz for Micromed.

All Neuralynx recordings were realized with Neuralynx Cheetah acquisition software.

2.5.3. Reference and patient ground

Macroelectrode reference: For recordings with the Micromed system (before Nov. 2018), a scalp reference electrode was used, placed as close as possible to the vertex of the head (Cz). For recordings with the Neuralynx system, the reference can be chosen from any of the recorded electrodes and can be different for macro and microelectrodes. For the macroelectrodes, when available, a contact in the white matter with a flat EEG signal and without epileptic activity, was selected. If such electrode contact was not available, the Cz scalp electrode was used. The latter was avoided when possible, because scalp electrodes are more likely to record muscle artifacts and to get detached from the skin, which introduces noise in all data.

Microelectrode reference: For each microelectrode, a microwire from the same bundle, with no MUA and no artifacts, was used as reference, to avoid injecting these activities in all electrodes. For model 1 and the large majority of model 2 and 3, one of the 8 microwires was selected. Using the un-insulated reference microwire for model 2 and 3 resulted most of the time in a higher noise level in the microelectrode signals, probably because the difference of impedance between the electrodes was too high. It was used only for 3 patients. Using a normal microwire as reference will enhance detection of very local activities but also eliminate all common activities recorded by the microwires, especially the slow components of the LFP that are generated from the averaged activity of a larger neuronal population. The un-insulated reference, on the contrary, will better preserve the slow components of the LFP but can also inject the same LFP activity in all microwires because of the difference of impedance and amplitude of signal captured by the electrodes. The impact on the LFP, whatever the wire used as reference, can vary depending on the distance between the microwires in the brain, which is unpredictable with the Behnke-Fried electrodes (Jurczynski et al., 2021).

Signal quality of microelectrodes was daily checked. If MUAs or artifacts appeared on all wires, which usually meant that the reference was

contaminated by those activities, another microwire of the microelectrode bundle was selected as a reference.

Ground: A scalp electrode on the collarbone was used for the patient's ground. Before November 2018, when 2 different amplifiers were used, the same patient's ground was used for both by using a jumper cable.

2.6. Data management

2.6.1. Storage

Microelectrodes are recorded at high sampling rate (32 kHz in our configuration) which can lead to an important amount of data to manage and store when acquired continuously for several weeks. A single channel recorded at 32 kHz for 2 h weighs almost 0.5 GB. In 2 to 3 weeks, a continuous recording of around 100 macro and microelectrodes, including 8 to 32 microwires accumulates 2 to 3 TB of data.

Because the research center (Paris Brain Institute) and the epilepsy unit are located on the hospital grounds in different buildings with separated network infrastructures, an optic fiber was extended from the epilepsy unit to the servers of the research center, allowing a direct data transfer since Feb. 2013. Every night, the data acquired by the Neuralynx system was transferred to the server at the Paris Brain Institute, allowing for a quick visualization and analysis by researchers. Before storage on the server, all data was pseudo-anonymized if not already done at the acquisition. All recorded data were segmented into files of 2 h maximum to optimize their reading access with the different visualization and analysis softwares. As Cheetah software did not allow segmentation without losing samples between files, recordings were usually launched for 24 h and segmented offline with Matlab software to 2 h without data loss. Data were organized by patients with standardized nomenclature and organization to facilitate access to the desired dataset. Acquisition settings, imagery and clinical information were added to each patient's folder. Access to the data was secured with personal ID and password, and obtained on demand for collaborators. Data acquired by the clinical softwares was stored and managed by the hospital IT infrastructure.

2.6.2. Electrode localisation and visualization

Within the EPILOC toolbox, two modules have been developed to localize implanted electrodes and their contacts spatially and anatomically. They were based on several image processing pipelines, using Brainvisa (Rivière et al., 2011, https://brainvisa.info/web/) and Freesurfer (http://surfer.nmr.mgh.harvard.edu/), that were built to: 1) compute anatomical models from the structural MRI preoperative sequence, 2) normalize this sequence on MNI template, 3) coregister pre- and post-operative sequences in the patient native space with the structural preoperative MRI as reference, using a block matching algorithm, 4) automatically localize depth sEEG electrodes on CT postoperative sequences, by segmentation of electrode artifacts present on the postoperative TDM and their classification using their distance to the theoretical trajectories planned on the stereotactic guidance device (ROSA or Leksell), 5) label all the contacts using the MNI atlases and the patient specific anatomical models. A first module allowed to check and correct, if necessary, potential mismatches of the automatic localization stage. The second module called EPILOC-VIEW created an interface that allowed users to navigate easily on a 3D scene, where all the results of different pipelines were merged. The user had the possibility to navigate among the different implanted electrodes and contacts and focus on each electrode by choosing a classical view or a view along the axis of the electrode, which was important to better identify the traces of the microelectrodes (Fig. 1). The structural image normalization allowed to report all the patient's data in the MNI space and visualize them in both native and MNI spaces. Microelectrodes were detected on the postoperative 3D CT scan. The superimposition with the pre-implantation MRI sequences allowed the identification of the individual anatomical localization. Their localization in the seizure onset zone (SOZ) was extracted from the clinical reports.

2.6.3. Signal visualization

It is often necessary to inspect the raw signal not only to check data quality and artifacts, but also to annotate pathological or physiological activities for further analyses. However, data acquired since 2012 was difficult to read with available software. Macro and microelectrodes signals were acquired at different sampling rates which is typically not supported in software for EEG visualization. Furthermore, before 2012 data were acquired on different amplifiers, and saved in different data files and formats. Data duplication due to conversion to different data formats becomes a storage issue with continuous recordings. In response to these issues, an in-house EEG/MEG software, MUSE (Ducorps et al., 2010) (Supp. Fig. 3), was updated to visualize macro and microelectrode signals directly from different file formats and at different sampling rates. For macro and microelectrode signals that were acquired on different amplifiers, the analog synchronization triggers were used offline to find the delay between the signals and to synchronize two visualization windows. When macro and microelectrode signals were acquired synchronously on the same Neuralynx system, all signals could be visualized at their original sampling rate. The MUSE software also gives the possibility to filter macro and microelectrodes separately at different frequencies and to annotate artifacts and events of interest (i.e. seizures, interictal activities, etc).

2.7. Noise / data quality

2.7.1. Room isolation and noise measurements

Because of their high impedance (Stacey et al., 2013), microelectrodes are more sensitive to artifacts than macroelectrodes. The most pervasive noise comes from the electrical recording environment, especially at 50/60Hz. The signal to noise ratio (SNR) can be insufficient if the electrical environment is too noisy, which in turn will prevent the detection of action potentials. The most effective way to reduce noise in the data is first to prevent or reduce it, e.g., by changing the electrical setup of the recording room. The hospital room used for the intracranial investigation was part of a building built in the 1960s. EMC-ZM (Electromagnetic Compatibility - Zero Method, Soleil et al., 1992, http://danielsoleil.com) measurements were performed and uncovered that the EEG recording room was full of noisy sources from electrical power distribution. Therefore, in 2014 a specific electrical installation, called "Low-Noise", was performed to approach 0 Vp and 0 Ap, i.e. no electrical noise (Fig. 5). This installation involved the followings:

- the creation of an isolated ground plane of reference made of a copper sheet of 0.3 mm thickness covering the floor of the room and itself protected by an antistatic coating;
- the electric power of the building, before arriving to the room, was isolated with a low capacitor coupling transformer whose output was a two-phase 230V rms, with its mid-point connected to the reference plane;
- all subsequent distribution of the current to the room outlets was filtered by low HF-losses capacitors until outlets of the room to obtain the Low-Noise. The two-phase and filtered power supply remove the electric radiation of the main cords;
- all outlet grounds of the room were shortetly referenced to the ground plane. All metallic objects (bed, table, chair, etc…) in the room were connected to the ground plane of reference when possible.

Noise measurements were done with a "Clean Energy Meter" (Hager, HagerGroup, Blieskastel, Germany) before and after the improvements. This measuring tool is a voltmeter that measures peak unreversed voltages after elimination of 50 Hz power supply with a high pass filter. Switched to an Ampere meter, it can be used to check that there is no current, even at 50 Hz, near the conductors connected to the isolated ground plane.

All the works were in accordance with NFC 15-100 and NFC 15-211 and the measurements were in line with IEC 61 000 -6 and -16.

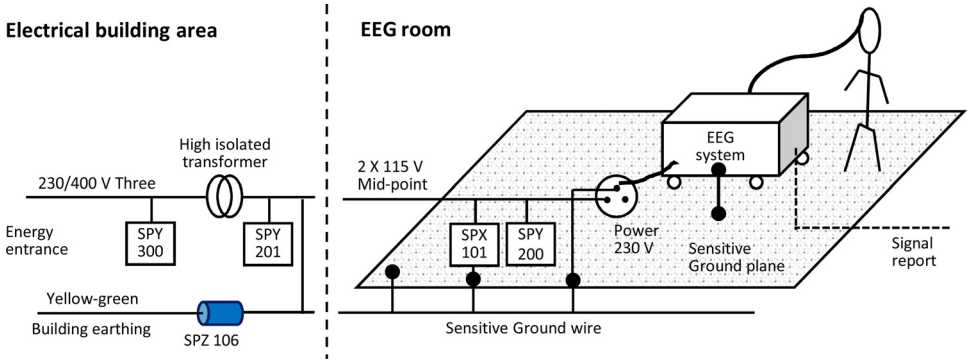

Fig. 5. Synoptic electrical diagram of the electrical installation in the patient's room. SPX 101: Hardening filter 2 phases. SPY 300: Capacitor bloc 3 phases 4.7 µF. SPY 200: Capacitor bloc 2 phases 4.7 µF. SPY 201: Capacitor bloc 2 phases 15 µF. SPZ 106: Magnetical bloc, hole 10 mm - Clean Energy HAGER.

Table 4
Description of main time periods of recording.

Time Period	Date	Recording system for macro-electrodes	Recording system for micro-electrodes	Electrical shielding of the room	Electrode model	Number of patients
1	Oct. 2010 - Jun. 2012	Neuralynx	Micromed	no	1	11
2	Nov. 2012 - Jul. 2014	Neuralynx + Micromed	Neuralynx + Micromed	no	1 or 2	14
3	Nov. 2014 - Oct. 2016	Neuralynx + Micromed	Neuralynx + Micromed	yes	1 or 2	14
4	Feb. 2017 - Oct. 2018	Neuralynx + Micromed	Neuralynx + Micromed	yes	3	11
5	Nov. 2018 - Sept. 2019	Neuralynx	Neuralynx	yes	3	6

2.7.2. Signal quality measures and statistics

In order to estimate the SNR of the microelectrode recordings, the root mean square (RMS) was calculated on 10 minutes of signal filtered between 300 and 3000 Hz, from 15 periods blindly selected without a priori on data quality but equally distributed in time, over the whole recording of each patient. No selection regarding the signal quality was done in order to keep an objective overview of the continuous recording and the possible quality variation in time.

According to the literature and our observations, low levels of noise increase the possibility to detect action potentials in the signal and the accuracy of the spike sorting (Buccino et al., 2020; Chaure et al., 2018; Wild et al., 2012). To test whether a decrease in noise was associated with an increase in action potential recordings, the presence of MUA was visually checked on filtered signals using MUSE software (300-300 Hz) and reported. The following measures were realized for each bundle: the number of wires recording at least once MUA along the 15 periods, referred as overall MUA; the number of wires recording MUA the first day of recording (day 0), after 1 week (day 6) and after 2 weeks (day 13), referred as time-dependent MUA. The first day of recording started the day following the implantation.

According to the improvement steps (new recording system, electrical shielding of the room, reinforced electrode model) of our recording procedure, five major time periods could be identified from 2010 to 2020 and are summarized in Table 4. Variation of RMS values and MUA quantification measured at the different time periods were evaluated using Generalized Linear Mixed Models (GLMMs).

RMS: For the RMS, a GLMM with identity link and normal distribution was used, with RMS values for each of the 15 distributed periods of each patient's wire as the dependent variable, the time period and the number of days after the first recording day as the fixed effects and the patients' ID with the wire's ID nested as the random intercept effects. In order to compare the proportion of extreme RMS values in each time period, they were identified as RMS values > Q3 + 1.5xIQR, with Q3 and IQR calculated on all RMS values, and a pairwise Fisher's exact test was performed between time periods and extreme RMS values identification. As RMS values were right-skewed, they were log10 transformed.

MUA: For the MUA, to test whether the overall MUA differed between time periods or was related to RMS values, two GLMMs with log link and Poisson distribution were performed, with the overall MUA quantification as the dependent variable, the time periods or the median RMS of each bundle as the fixed effects and the patients' ID as the random intercept effects. Lastly to test whether the number of wires recording MUA differed between time periods and days of recording, a GLMM with log link and Poisson distribution was performed, with the time-dependent MUA quantification as the dependent variable, the time periods and the day of recording as the fixed effects and the patients' ID as the random intercept effects. To test whether there was a difference between the time periods according to the day of recording, the interaction between the time periods and the day of recording was added as a fixed effect in the previous model.

For RMS and MUA, type II Wald chi-square tests were used to test main effects and interactions and post hoc pairwise comparisons were carried out when appropriate. Mean difference estimates (MDE) ± standard errors (SE) and mean ratio estimates (MRE) ± SE were reported for post-hoc comparisons of RMS and MUA respectively. For all analysis and figures, RMS values from the microwires used as reference were excluded.

The signal measures were calculated with Matlab (MATLAB. (2019) *version* 9.7.0 *(R2019b)*. Natick, Massachusetts: The MathWorks Inc.) and statistical analyses and figures were achieved using R 4.1.2 (R Foundation for Statistical Computing, Vienna, Austria. URL "https://www.R-project.org".)) and lme4 package (v1.1-27.1, Bates et al., 2014, p. 4) for GLMM fit, emmeans package (v1.7.2, Lenth, 2020) for post-hoc comparisons and model representation, optimx package (v2021.1.12, Nash, 2011) for GLMM convergence, and RVAideMemoire package (v0.9.81, Hervé) for pairwise Fisher's exact test .

2.8. LFP-MUA/SUA pipeline analysis of epileptic events

To illustrate the type of analysis that can be performed on epileptic events, this section presents a procedure developed in our lab to investigate the firing behavior of neurons during interictal epileptic spikes (IEDs), which are brief paroxysmal electrographic discharges that can be observed visually on EEG. Microelectrode wires were first selected, based on whether they showed MUA and IEDs. Artifacts and IEDs were annotated manually on the basis of visual observation of the microelectrodes. All annotations were done with MUSE, a software developed in-house to allow the visualization of both macro and micro electrodes. Spike sorting was then done using Spyking Circus (Yger et al., 2018), according to the procedure outlined in detail in their reference docu-

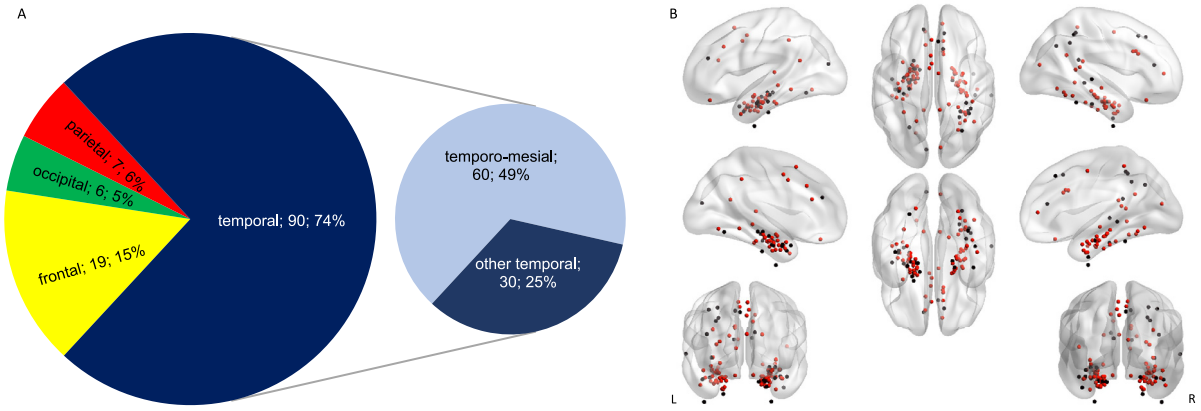

Fig. 6. Microelectrode localization. A. Distribution diagram of the electrode localizations with a detailed focus for the temporal lobe. The temporo-mesial region includes: hippocampal formation, amygdala, parahippocampus. The first number near the brain region's name indicates the number of microelectrodes in the corresponding region, the 2d number indicates the percentage of microelectrodes. **B.** 3D MNI normalized localizations of the microelectrodes. Each dot is a microelectrode bundle. Red dots correspond to microelectrode bundles that recorded MUA and black dots correspond to microelectrode bundles that did not record MUA. The 3D figure was realized using BrainNet viewer (www.nitrc.org). *Note that some dots appear outside of the brain because of the imprecision of the MNI normalization, especially for electrodes at the border of the temporal lobes where the MRI quality is not as good as for the rest of the brain.*

mentation (https://spyking-circus.readthedocs.io/en/latest/) and reference article (Yger et al., 2018) . In short, Spiking Circus uses a combination of density-based clustering and template matching algorithms to automatically cluster the detected action potentials into putative single units. Data is temporally whitened, and action potentials (APs) are automatically detected at 6 (or higher) median absolute deviations (MAD) of high-pass filtered (> 300 Hz) signal. APs that occurred during annotated artifacted periods were ignored, their inclusion would affect the spike sorting accuracy. Clusters that were not stable across the recording were discarded from further analysis. Clusters were further evaluated whether they reflected putative single-unit activity (SUA) or multi-unit activity (MUA) based on their inter-spike-interval (ISI), the percentage of refractory period violation, the consistency of their firing rate and amplitude over time, and their waveform morphology. IEDs were automatically aligned according to their cross-correlation. Average LFPs and spike times were then time-locked to the IEDs and plotted on the same time-axis. The analyses pipeline was implemented using custom MATLAB scripts (https://github.com/stephenwhitmarsh/EpiCode), and used FieldTrip (Oostenveld et al., 2011), a MATLAB (The Mathworks Inc., Natick, Massachusetts) toolbox for MEEG and spike analyses.

3. Results

3.1. Database description

From October 2010 to September 2020, 56 patients (31 women; age: mean = 33 years, range:18-60; duration of epilepsy: mean = 16 years, range:4-40) were implanted with a total of 122 microelectrode bundles (range: 1-4 per patient). Electrodes were mostly localized in the temporal lobe (n=90; 74%), with a predominance in the mesial temporal cortex (n=60), including hippocampal formation (n=31), amygdala (n=14), parahippocampus (n=6). Microelectrodes were also placed within frontal (n=19, 15%), parietal (n=7, 6%) and occipital (n=6, 5%) lobes (Fig. 6A). Most microelectrode bundles were in gray matter or lesioned tissue (n=99; 81%), but some spread in the white matter (n=4; 3%) or in extraparenchymal regions (n=13; 11%). In the temporal lobe, the proportion of microelectrodes in extraparenchymal regions was 6/22 for amygdala, 2/44 for hippocampal formation, and 3/9 for temporo-basal regions.

Signal from microelectrodes was recorded from 55 patients and 119 microbundles; one patient at TimePeriod 1 could not be recorded for technical reasons. For the first 10 patients from TimePeriod 1, microelectrodes were recorded a few hours (1-4 h) per day, for 10 days on average, with a total duration of 14.5 h on average. For the next 45 patients, microelectrodes were recorded continuously for an average of 16.2 days (min = 5 days, max = 27 days). Twenty-seven among the 122 microelectrodes were located in the SOZ (Fig. 6B).

During TimePeriod 1, seizures could be recorded with microelectrodes for 50% of the patients with a total of 33 seizures (5/10 patients, with 1 to 17 seizures/patient). Microelectrodes were in the SOZ for 2 patients. During TimePeriod 2 to 5, seizures could be recorded with microelectrodes for 91% of the patients (41/45 patients, with 2 to > 50 seizures per patient). Microelectrodes were in the SOZ for 16 patients.

3.2. Signal quality measures

3.2.1. Electrical noise in the room

Room measurements before and after the new electrical installation revealed that the noise level in the patient's room decreased from values around 8V High Frequency (HF) peak-to-peak to less than 0.1 V peak-to-peak, corresponding to a 35 dB of reduction .

3.2.2. Data SNR

The LMM investigating RMS differences over recording time periods revealed a significant effect of the time period (Chi^2 = 99.29, p<0.001, Fig. 7, Table 5 for descriptive statistics). Compared to TimePeriod 2, RMS values were significantly lower during TimePeriod 1 (MDE ± SE = -0.50±0.06, p<0.001), when micro and macroelectrodes were recorded separately, and during TimePeriod 3 (MDE±SE = -0.33±0.06, p<0.001), TimePeriod 4 (MDE±SE = -0.47±0.06, p<0.001) and TimePeriod 5 (MDE±SE = -0.46±0.07, p<0.001) after the room has been electrically isolated. There was also a significant difference between TimePeriod 1 and 3, with lower values during TimePeriod 1 (MDE±SE = -0.17±0.06, p=0.037), but no significant difference between the other time periods (p>0.05). The difference between TimePeriod 3 and 4 was not significant but the median RMS value was higher during TimePeriod 3. The number of outliers differed between all time periods (pairwise Fisher's exact test, all p<0.001, Table 5 for descriptive statistics) apart between Time Period 4 and Time Period 5. The period with less outliers was Time Period 1, followed by Time Period 4 and 5, Time Period 3 and Time Period 2.

Moreover the LMM revealed a slight but significant increase of the RMS over days of recordings (estimate±SE = 5.53e-03±6.23e-04, Chi^2 = 78.77, p<0.001, Supp. Fig. 4). Individual data are presented in

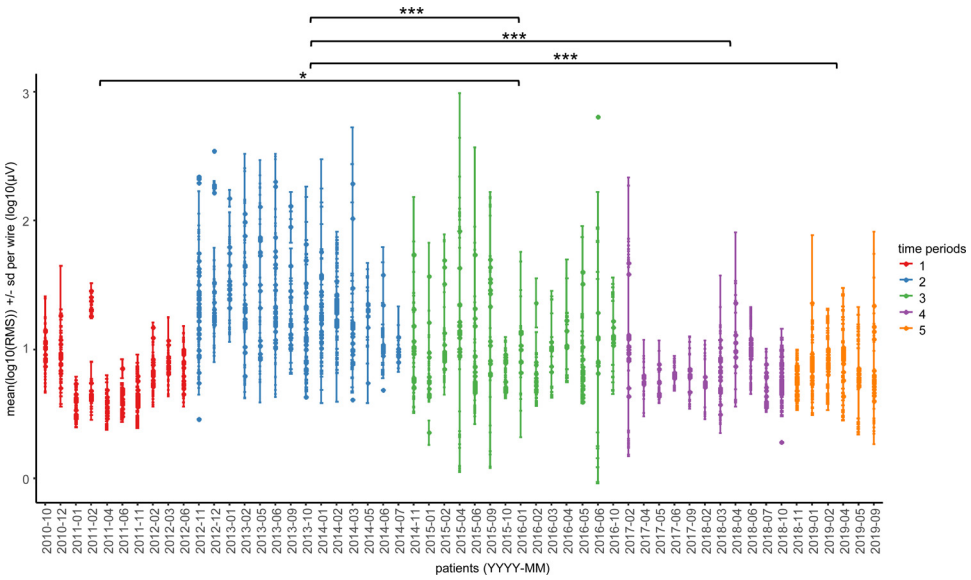

Fig. 7. RMS per wire and day for each patient. Each dot represents the mean of RMS values measured over days for each wire. Note that the y axis is expressed on a log10 scale, values of 1, 2 and 3 corresponding respectively to 10µV, 100µV and 1000µV. Dots are plotted according to the log10(RMS) mean value and the patient ID expressed in year-month (YYYY-MM). Bars represent the standard deviation of the log10(RMS) values of each wire. The color code distinguishes the 5 time periods (red: TimePeriod 1, blue: TimePeriod 2, green: TimePeriod 3, purple: TimePeriod 4, orange: TimePeriod 5). The patient's room was electrically cleaned between TimePeriod 2 and TimePeriod 3. The electrode model was changed to the reinforced model 3 between Time Period 3 and Time Period 4. Significant differences between time periods are indicated with stars (*: 0.05 > p < 0.01; **: 0.01 > p < 0.001; ***: p < 0.001).

Table 5
Descriptive statistics of each time period.

Time Period	RMS (µV)						MUA (nb wires/bundle)			
	N total	Outliers		Median	Q1	Q3	N total	Median	Q1	Q3
		N	%							
1	1527	3	0.20	6.30	4.48	9.15	19	2	0	4
2	3497	412	11.78	16.96	9.80	36.21	34	0.5	0	2
3	2718	101	3.72	6.45	4.73	11.72	26	3	0.25	4.75
4	2336	33	1.41	5.87	4.73	8.10	20	3	1	6
5	1654	34	2.05	5.82	4.53	8.26	15	4	1.5	5.5

Supp. Fig. 5. A GLMM with the interaction between recording day and the patient ID as the fixed effects precised significant positive correlation between RMS and days of recording for 25/55 patients, distributed in all time periods. The correlation was not significant for 19/55 patients and significantly negative for 11/55 patients.

3.2.3. MUA

For 70% of recorded microelectrode bundles (82/119), at least 1 wire from the microelectrode bundle showed MUA, with an average of 3 wires per bundle. The proportion of bundles recording MUA differed between time periods and reached 70.1 %, 50 %, 73.1 %, 85 % and 80 % for TimePeriod 1 to 5 respectively.

As can be observed on Fig. 8A, the relation between the RMS values and the number of wires recording MUA at least once was not linear. The maximum number of wires recording MUA was observed for RMS value around 7.4 µV. Above 7.4 µV the number of wires recording MUA decreased when RMS values increased, while below 7.4 µV the relation was inverted. A first GLMM focusing on RMS values > 7.4µV and testing the relation between the number of wires recording MUA and the RMS values, confirmed a significant negative impact of high RMS values on the number of wires per bundle recording MUA (estimate±SE = -0.07±0.03, Chi^2 = 47, p=0.034). A second GLMM focusing on RMS values < 7.4 and testing the relation between the number of wires recording MUA and the RMS values, confirmed a positive correlation (estimate±S = 0.47±0.08, Chi^2 = 34.27, p<0.001).

The GLMM testing whether overall MUA differed between time periods revealed a significant time period effect (Chi^2 = 16.52, p=0.002, Fig. 8B, Table 5 for descriptive statistics). There were significantly less wires per bundle recording MUA during TimePeriod 2 than during TimePeriod 3 (MRE)±SE = 0.42±0.12, p=0.016), TimePeriod 4 (MRE± SE = 0.34±0.11, p=0.007) and TimePeriod 5 (MRE± SE = 0.33±0.11, p=0.006).

The GLMM testing the time-dependent MUA revealed a significant effect of the time period (Chi2 = 17.96, p=0.001) and of the day of MUA measure (Chi2 = 57.59, p<0.001). Significantly less wires per bundle recorded MUA during TimePeriod 2 compared to TimePeriod 4 (MRE±SE = -1.53±0.40, p=0.001) and 5 (MRE±SE = -1.48±0.44, p=0.007). The number of wires recording MUA significantly differed between all days of recordings (day0 vs. day6: (MRE±SE = 1.62±0.19, p=0.001, day6 vs. day13: (MRE±SE = 1.97±0.33, p=0.002, day0 vs. days13: (MRE±SE = 3.19±0.51, p<0.001, Fig. 8C). The introduction of the interaction between the time periods and the day of MUA measure as fixed effects in the model did not reveal any significant interaction (Fig. 8C).

Interestingly, for 52 bundles, the total number of wires recording MUA at least once during the whole recording period, was higher than the number of wires recording MUA the first day of recording, reflecting the fluctuation from day to day of the presence of MUA on wires (see Supp. Fig. 3).

No MUA were recorded in 37 microbundles. For the majority of cases, this could be attributed to a localization outside gray matter, i.e. extraparenchymal (12 bundles), white matter (3 bundles), or a failure in the extrusion from the macroelectrode (4 bundles were not visible on the CT scan). For 8 bundles, the mean RMS was high (> 10µV). Finally, for 9 bundles there was no clear reason for the lack of MUA, as they were in the gray matter with RMS values < 5 µV.

As one of our objectives was to record as many seizures as possible with MUA, we looked at the number of patients for whom it was possible to record seizures with MUA. For 33 patients, we could record at least 1 seizure (range 1 to 10) with MUA on at least one microelectrode signal. Those 33 patients correspond to 40% of patients during TimePeriod 1,

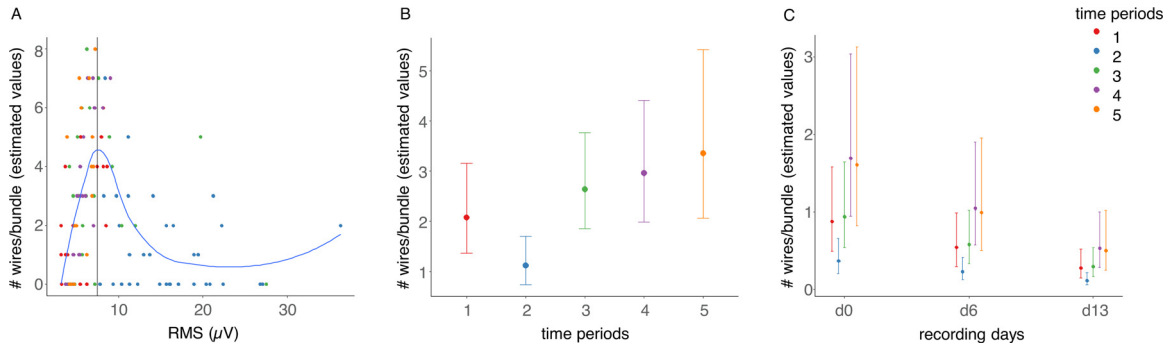

Fig. 8. Number of wires per bundle recording MUA. A. Representation of the number of wires per bundle recording at least once MUA during the whole recording, in relation to the median of RMS values measured on all wires of the bundle. The blue line fits the data with the LOESS method which uses local averaging. The vertical black line is plotted at the peak of the fitting line. **B.** Representation of the estimated marginal means of the number of wires per bundle recording at least once MUA during the whole recording for each time period given by the GLMM. Bars represent low and high 95% confidence intervals. **C.** Representation of the estimated marginal means of the number of wires per bundle recording at least once MUA values for each time period and day of recording (0-6-13) given by the GLMM. Bars represent low and high 95% confidence intervals. For all plots each dot represents a bundle and the color code distinguishes the 5 time periods (red: TimePeriod 1, blue: TimePeriod 2, green: TimePeriod 3, purple: TimePeriod 4, orange: TimePeriod 5). Significant differences between time periods are indicated with stars (*: $0.05 > p < 0.01$; **: $0.01 > p < 0.001$; ***: $p < 0.001$).

but with few seizures per patient, 28% of patients during TimePeriod 2, and 76% of patients during TimePeriod 3 to 5. Among those 33 patients, 12 had the microelectrodes recording MUA localized in the SOZ.

3.3. Example of analysis pipeline for long-term continuous recording of epileptic activity

The continuous and long-term recordings described here allows for manual or automatic annotation of epileptic events during active and passive wake state, as well as during sleep. Fig. 9 gives an example of the analysis pipeline described in the method (Section 2.8). Epileptic spikes were visible on both macro- and microelectrodes (Fig. 9A & B). The high-passed signal of the microelectrode showed action potentials, i.e MUA (Fig. 9C). Spike-sorting analysis isolated two different single neurons, i.e SUA (red and blue), with different morphologies (Fig. 9F) and firing properties (as noted, by the histogram of their inter-spike intervals; Fig. 9G). The firing rates of both neurons correlated with the LFP of the IEDs (Fig. 9D & E).

4. Discussion

During the last 10 years, we collected a database of 119 microelectrode recordings in patients with epilepsy. Most microelectrodes were implanted in mesial temporal regions, consistent with the predominance of temporal epilepsies (Blumcke et al., 2017). Our post-implantation imaging analysis also revealed that most of the microelectrodes were in gray matter as expected, but some were in white matter or meninges. This mistargetings can be related to our implantation strategy: the deepest macrocontact is placed in the mesial cortex and microwires must extend from there toward the inner part of the brain. During the trajectory planning, the estimated length for the microwires always comprises a margin of error of some mm, in case of potential deviation of the macroelectrode trajectory during the implantation. However, more deviation can occur and prevent the microelectrode from reaching the targeted localization. We observed more mistargetings of gray matter in some cerebral regions, such as amygdala, compared to other regions such as hippocampus, probably because the volume of gray matter beyond the tip of the electrode is smaller in amygdala. Nevertheless, the addition of microelectrodes did not increase the risk of hemorrhages and infectious complications (Mathon et al., 2015).

The analysis of the noise level and the presence of MUA on our microelectrode recordings showed a progressive improvement related to several technical changes. The analyses were performed on blindly selected files equally distributed along the whole recording, in order to have the most objective overview of noise levels. The electrical insulation of the patient's room came out as a major effect, and the use of the reinforced micro-bundle had smaller but not negligible consequences. Most RMS values of the filtered microelectrode signal from the last time periods (i.e., our current recording configuration), were relatively low. For Time Period 4 and 5, more than 85% and nearly 70 % of the measures were < 7.4 μV during the 1st and 2d week respectively, while they were below 10 % for Time Period 2. The number of wires per bundle recording MUA significantly increased over time periods—from 2010 to 2020. The quality improvement of the data was efficient from the first days of the recording and allowed to keep a better quality (lower RMS and more wires with MUA) until the end of the recording. The reduction of RMS values in our data increased our possibilities to record MUA and therefore the probability to better isolate SUA through spike sorting (Buccino et al., 2020; Chaure et al., 2018; Wild et al., 2012). This relation between MUA and SUA was indeed observed in several analyses conducted on our data. The more MUA were present in the recordings, the more SUA could be isolated. According to Fig. 8A, it seems that reaching a RMS < 10 μV is important to obtain a SNR high enough to catch action potentials. The fact that we observed less MUA for RMS below 5 μV can probably be explained by a very low electrical and physiological noise, i.e. the lack of MUA on the signal contributes to the RMS reduction of the filtered signal. Interestingly, during our first microelectrodes recordings (TimePeriod 1), when microelectrodes were recorded separately from the macroelectrodes and for only a couple of hours per day, we obtained lower RMS, more MUA than during TimePeriod 2 and less outliers than during all other time periods. This might be explained by the presence of researchers during the whole recording, systematically trying to reduce noise, i.e. by shielding all cables and starting to record only when the noise level was low. The transition to a single amplifier for macro and microelectrodes (TimePeriod 2) was first associated with a decrease of signal quality. However the decrease of RMS values during TimePeriod 2 reveals the impact of the improvements realized at all steps from implantation to recordings. The significant difference in RMS values between TimePeriod 2 and TimePeriod 3 highlights the importance of the electrical insulation of the patient room, whose financial cost was balanced by the major noise reduction. However, modifying the electrical installation is not always possible and it will also not prevent some electrical noise sources. Shielding cables to prevent surrounding electromagnetic interference and avoiding ground loops is essential (see Misra et al., 2014, for details). We could observe 50/60Hz noise reduction in the microelectrodes by covering their poorly shielded tail with a conductive tissue grounded to the patient (Stretch conductive fabric, Less EMF Inc., Latham NY 12110, USA). Furthermore, like

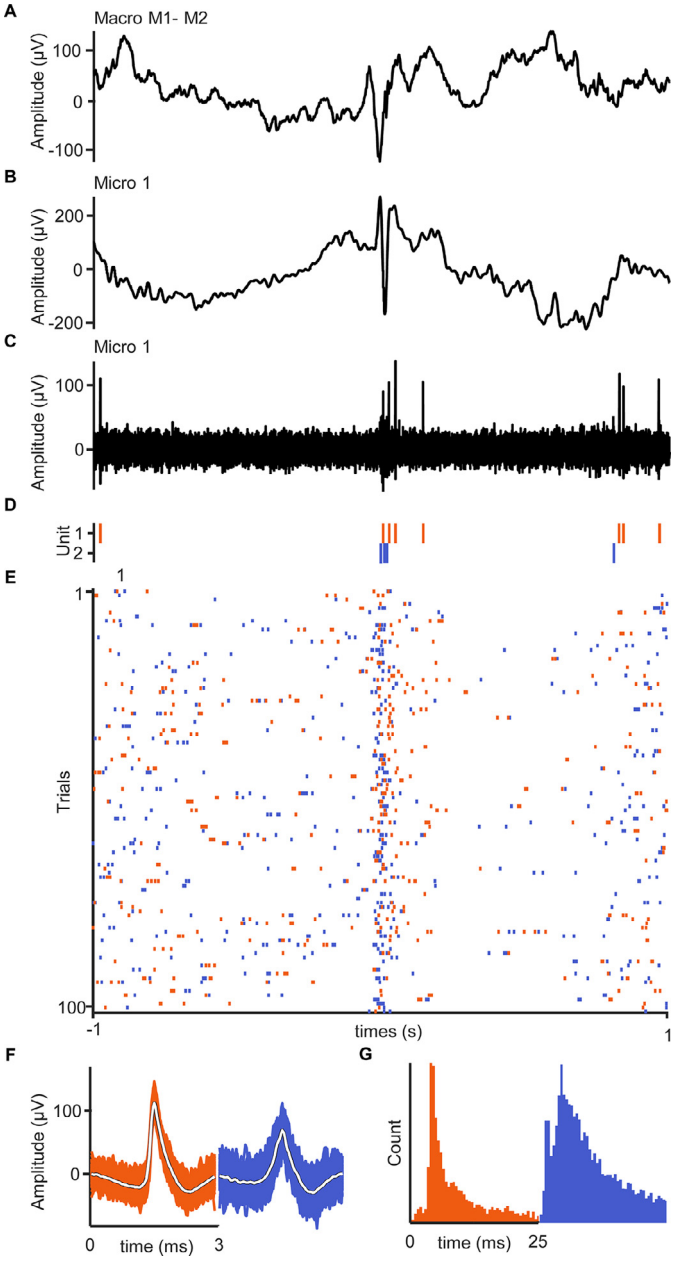

Fig. 9. Example of single units time-locked to the LFP of IEDs. A. IED recorded by a macro contact. The macroelectrode iEEG signal is shown on a bipolar montage (M1-M2). **B.** Same IED as in A recorded by a micro wire (Micro 1) at the tip of the macroelectrode represented in A, the signal is low-pass filtered at 50 Hz. **C.** Same signal as B but high-pass filtered at 500Hz. The filtered signal shows action potentials (multi-units activity). **D.** Spike sorting of Micro 1 signal resulted in a separation of action potentials into two different putative single units (red and blue color code). Red and blue lines represent the occurence in time of action potentials of each unit. **E.** Raster plot of 100 IEDs recorded by Micro 1. Action potential times of each unit (red and blue) were time-locked to the IEDs, showing clear synchronization. **F.** Action potential waveforms of each unit: 1000 random time courses with superimposed average. **G.** Inter-spike-interval histogram of each unit.

for all electrophysiological recordings, any electrical device plugged in an outlet that touches the patient, the bed/chair where the patient is sitting, or the connectors and tether cables, will introduce 50/60Hz noise and should be avoided. Therefore, if the patient needs to use a computer or his phone, they should preferably run on battery. However, even on battery, a laptop can be a source of noise for the microelectrodes when the patient touches the keyboard. One solution, especially for cognitive tasks where responses are mandatory, is to use optical cables to connect to button response boxes. Wireless keyboards or mouses might also work, but should first be tested regarding the responses delays and jitters. The patient's bed, if it is electrically motorized, can also be a source of noise. If it is the case, unplugging or using a manual bed should be considered. We also experienced that keeping a loose scalp electrode connected to the Neuralynx amplifier was another source of slow wave artifacts for all electrodes connected to the same input board of 32 channels. Hanging scalp electrodes have the impedance of the headbox or system input and behave like an antenna in the air that will pick up the noise in the environment.

The reference is also important for reducing noise levels. Even if references can always be changed offline, the use of the best reference during acquisition enhances the chances to have a good signal. For example, if the reference is damaged and sensitive to movements/noise and is likely to saturate, then all signals will saturate and it will not be possible to gain signal by offline re-referencing. A good reference also contributes to on-line estimates of the signal quality, so that the recording setup can be adapted when necessary. Because we often observed, like Misra et al 2014, an increase in noise level with the un-insulated wire, we mostly preferred a normal microwire for model 2 and 3, despite the impact on the LFP. This is not the choice of all centers recording with microelectrodes, probably because of the possibility to re-reference off-line prior spike-sorting if needed. Several re-referencing techniques can be used like using a local reference or the average of all wires. In addition to those classical techniques, Jurczynski and colleagues (Jurczynski et al., 2021) also proposed an adaptive version of the zero-reference method. The impact of the un-insulated wire that differs from one patient to another would need further investigation, as well as the impact on unit recordings and spike sorting.

Any damage of the microwire will increase not only the impedance of the electrode (Misra et al., 2014) and 50/60Hz noise, but also artifacts due to movement. Damage can happen at any time between the surgery and the end of recording, especially when the electrode was manipulated and could explain a decrease in data quality. Therefore, we established a procedure from the surgery to the end of recording (Tables 1 & 2), where at each step, electrodes are manipulated carefully: by the neurosurgeons when they cut the wires and insert them into the macroelectrode, by the nurses when they wrap the head with the bandage, and by the technicians when they connect the tails to the connectors. Interestingly, we observed less extreme RMS values (less outliers), probably related to less damage of wires, after switching to the more resistant model of the Behnke-Fried microelectrode. Noisy channels were in general present from the beginning of the recording, revealing a degradation of the electrode more likely to occur between the surgery and the beginning of the recording than during the recording. The reinforcement of the electrode seems therefore to decrease the risk of breaking and improves the quality of the recordings during the whole acquisition.

We also observed that the RMS values slightly increased over time and that this was associated with less MUA recordings. The increase in RMS might be due to an increase in the microwires' impedance, as observed on another electrode model (Despouy et al., 2020). The loss of MUA could also be due to the inflammatory reaction around the microelectrodes, which insertion in the neural tissue can cause gliosis leading to the loss of sensitivity of the recording (Babb et al., 1973; Polikov et al., 2005). Despite the reduced number of wires recording MUA at the end of the recording, it often happened that MUA appeared on new wires or reappeared after a 'silent' interval. This fluctuation would need further exploration. However we hypothesize that it might be due to a slight movement of the electrode or the brain, as previously described (Babb et al., 1973), allowing the wire to record from other neurons than the previous ones. Alternatively, it might be due to changes in impedance due to movements of the electrode tail.

Improved quality of continuous and long-term recording from microelectrodes, increases the possibility to record seizures with micro-

Table 6
Summary of main guidelines.

Main guidelines
Very careful manipulation of the microelectrodes at all steps (Figs. 2 & 3 /Tables 1 & 2)
Prefer the most robust Ad-Tech microelectrode if you use Ad-Tech electrodes (Section 2.5.1)
If possible, the recording room should be shielded or have a clean electrical installation (Section 2.7.1)
Shield as much as possible (cables, electrode tails; Section 4.)
Avoid ground loops (Section 4.)
No electrical device plugged in an outlet should touch directly or indirectly the patient (Section 4.)
If possible, reduce to a single amplifier. If not, both amplifier should be connected to the same outlet and grounded to the same patient's ground (Section 2.5.2)
The patient should never be connected to the electrical ground for safety reasons
Do not connect scalp electrodes to Neuralynx if they are not pasted to the patient' skin (Section 4.)
Prepare an appropriate IT infrastructure in case of long-term recording of microelectrodes, to collect the high amount of data generated

electrodes, which is a crucial requirement to study ictogenesis and the cellular mechanisms related to seizures emergence. Our data shows that it was indeed necessary to record continuously from macro and microelectrode, in order to capture seizures whose occurrence is unpredictable. A first analysis of 38 seizures from 9 patients, recorded by microelectrodes within the SOZ showed that neuronal spiking activity at seizure initiation was highly heterogeneous and not hypersynchronous (Lambrecq et al., 2017). However, recording from the seizure-onset-zone remains a challenge, which by definition, is unknown at the beginning of the intracranial investigation. In addition, Behnke-Fried micro-macroelectrodes can only record deep structures like the mesial temporal structures, but are not tailored for sampling neocortical structures. On the contrary, cortical multielectrode arrays (Utah arrays) provide coverage of neocortical structures, but provoke cortical damage and can only be used on structures that will be surgically removed. Hybrid electrode models with microwires protruding between macrocontacts, e.g. DIXI tetrodes (MICRODEEP® Micro-Macro Depth Electrode), are a good way to record units in more superficial cortical areas (Despouy et al., 2020, 2019).

The number of wires per bundle that recorded MUA remained quite low, around 3 out of 8 (range 0-8), and did not seem to be only a SNR issue as very low RMS with no MUA could be observed. The absence of MUA might also be related to the distance between the wires and active neurons. One solution would be to adapt the length of the microwires, once implanted in the brain in order to try to get closer to neurons if no MUA is recorded. As far as we know, DIXI tetrodes are the only electrode model proposing such a technology that allows to pull out the wires up to 2 mm. Beside, another interesting feature of DIXI microelectrodes is their *tetrode* configuration rather than single wires, which should allow better separation of single units based on the spatial distribution of action-potential recordings. Most unsupervised spike sorting software can use the tetrode configuration to separate detected action potentials in different units (Buccino et al., 2020).

Keeping 3 weeks of continuous recording, including microelectrodes at high sampling rate, generates a large amount of data to be stored, backuped, analyzed and shared. This is only possible with an efficient IT infrastructure, allowing high storage capacity but also fast and secured data access. As an example, we generate around 2 TB of data per patient. In addition to the storage capacity, there is also the question of data organization, including all the metadata related to the patient and the recordings. Each patient investigation is different in terms of electrode localisation, SOZ, medication and all those metada are necessary to analyze the electrophysiological data, to study epilepsy or cognitive processings. A structured database becomes essential when the number of patients increases. We therefore developed a secure survey and database that can include clinical information, electrode localization and technical settings. Another possibility, which is not mutually exclusive, is to adopt the BIDS dataformat (Holdgraf et al., 2019), that is standardized, adapted for data sharing and gives the possibility to add metadata for each recording. Finally, a good organization combined to a suitable analysis pipeline (see Section 2.8 and Fig. 9), a powerful spike sorting tool tailored for long-term data (Buccino et al., 2020; Chaure et al., 2018; Niediek et al., 2016; Rey et al., 2015; Wild et al., 2012, Yger et al. 2018) and high computational capabilities are essential keys to achieve analyses of large amounts of collected data.

5. Conclusion and perspectives

We showed that it is feasible to record high quality, long-term and continuous microelectrode signals *in vivo* in patients with epilepsy. Our procedure allows the recording of both LFP and single neurons activity during physiological (as wakefulness and sleep) and pathological (as interictal epileptiform discharges and seizures) periods. We shared our experience to improve the quality of these recordings and we proposed several technical guidelines (Tables 1, 2 and 6), that are complementary to other methodological papers on microelectrodes recordings (Minxha et al., 2018; Misra et al., 2014 for Behnke-Fried electrodes; Despouy et al., 2020 for Dixi macro-microelectrodes). We described in detail head wrappings after the surgery that are crucial steps in the electrode manipulation, and quantify noise level depending on acquisition setup and environnement.

Studying ictogenesis in focal epilepsies using intracerebral microelectrodes is faced with a great number of specific challenges: (i) to record in the actual SOZ, (ii) to record unitary activity during seizures, (iii) to follow the same neuron over time during different epileptic events, and (iv) to be faced to great interindividual variability. In the future, the increased availability of microelectrode technology and shared recording-protocols will increase the pool of human microelectrode data among neuroscientists and help overcome these difficulties. Progress will likely come from additional technical advancements, like the development of a mobile microelectrodes which could be moved further in or out when unitary activities are lost, or the development of non-penetrating cortical microelectrode arrays (Khodagholy et al., 2015). Microelectrodes show great potential in the field of epilepsy (Chari et al., 2020). In the coming decades, we expect that they will increasingly contribute to deciphering the cellular mechanisms of seizure generation and to establish new markers of the epileptogenic focus.

CRediT author statement

Conceptualization: Katia Lehongre, Virginie Lambrecq, Vincent Navarro

Methodology: Katia Lehongre, Virginie Lambrecq, Stephen Whitmarsh, Vincent Navarro

Software: Katia Lehongre, Stephen Whitmarsh, Valerio Frazzini, Sara Fernandez-Vidal, Jean-Didier Lemarechal, Dominique Hasboun,

Formal analysis: Katia Lehongre, Virginie Lambrecq, Stephen Whitmarsh, Valerio Frazzini, Marion Houot

Resources: Katia Lehongre, Virginie Lambrecq, Valerio Frazzini, Louis Cousyn, Daniel Soleil, Bertrand Mathon, Stéphane Clemenceau, Dominique Hasboun, Claude Adam, Vincent Navarro

Writing - original draft: Katia Lehongre, Virginie Lambrecq, Stephen Whitmarsh, Valerio Frazzini, Louis Cousyn, Daniel Soleil, Sara Fernandez-Vidal, Bertrand Mathon, Jean-Didier Lemarechal, Stéphane Clemenceau, Dominique Hasboun, Claude Adam, Vincent Navarro

Writing - review & editing: Katia Lehongre, Virginie Lambrecq, Stephen Whitmarsh, Valerio Frazzini, Louis Cousyn, Daniel Soleil, Sara Fernandez-Vidal, Bertrand Mathon, Marion Houot, Jean-Didier Lemarechal, Dominique Hasboun, Claude Adam, Vincent Navarro

Supervision & Funding acquisition: Vincent Navarro

Declaration of Competing Interest

D. Soleil is the manager of the CEMS society. The other authors have no conflict of interest in relation with this work.

Acknowledgments

This work received support from the “Investissements d’avenir” program (ANR-10-IAIHU-06), and from the Fondation Assistance Publique Hôpitaux de Paris (EPIRES – Marie Laure PLV Merchandising). We thank all the nurses and technicians for their involvement in the microelectrode recordings. We thank Charlotte Lebaz, Pauline Marijon, Corinne Lascaut, Ghislaine Therme, Nadège Manelle and Sabine Dedenis for their kind participation in the realization of the pictures for the Figs. 2 and 3.

Supplementary materials

Supplementary material associated with this article can be found, in the online version, at doi:10.1016/j.neuroimage.2022.119116.

References

Alvarado-Rojas, C., Lehongre, K., Bagdasaryan, J., Bragin, A., Staba, R., Engel, J., Navarro, V., Le Van Quyen, M., 2013. Single-unit activities during epileptic discharges in the human hippocampal formation. Front. Comput. Neurosci. 7, 140. doi:10.3389/fncom.2013.00140.

Axelrod, V., Rozier, C., Malkinson, T.S., Lehongre, K., Adam, C., Lambrecq, V., Navarro, V., Naccache, L., 2019. Face-selective neurons in the vicinity of the human fusiform face area. Neurology 92, 197–198. doi:10.1212/WNL.0000000000006806.

Babb, T.L., Carr, E., Crandall, P.H., 1973. Analysis of extracellular firing patterns of deep temporal lobe structures in man. Electroencephalogr. Clin. Neurophysiol. 34, 247–257. doi:10.1016/0013-4694(73)90252-6.

Babb, T.L., Crandall, P.H., 1976. Epileptogenesis of human limbic neurons in psychomotor epileptics. Electroencephalogr. Clin. Neurophysiol. 40, 225–243. doi:10.1016/0013-4694(76)90147-4.

Bates, D., Mächler, M., Bolker, B., Walker, S., 2014. Fitting Linear Mixed-Effects Models using lme4. ArXiv14065823 Stat.

Blumcke, I., Spreafico, R., Haaker, G., Coras, R., Kobow, K., Bien, C.G., Pfäfflin, M., Elger, C., Widman, G., Schramm, J., Becker, A., Braun, K.P., Leijten, F., Baayen, J.C., Aronica, E., Chassoux, F., Hamer, H., Stefan, H., Rössler, K., Thom, M., Walker, M.C., Sisodiya, S.M., Duncan, J.S., McEvoy, A.W., Pieper, T., Holthausen, H., Kudernatsch, M., Meencke, H.J., Kahane, P., Schulze-Bonhage, A., Zentner, J., Heiland, D.H., Urbach, H., Steinhoff, B.J., Bast, T., Tassi, L., Lo Russo, G., Özkara, C., Oz, B., Krsek, P., Vogelgesang, S., Runge, U., Lerche, H., Weber, Y., Honavar, M., Pimentel, J., Arzimanoglou, A., Ulate-Campos, A., Noachtar, S., Hartl, E., Schijns, O., Guerrini, R., Barba, C., Jacques, T.S., Cross, J.H., Feucht, M., Mühlebner, A., Grunwald, T., Trinka, E., Winkler, P.A., Gil-Nagel, A., Toledano Delgado, R., Mayer, T., Lutz, M., Zountsas, B., Garganis, K., Rosenow, F., Hermsen, A., von Oertzen, T.J., Diepgen, T.L., Avanzini, G.EEBB Consortium, 2017. Histopathological findings in brain tissue obtained during epilepsy surgery. N. Engl. J. Med. 377, 1648–1656. doi:10.1056/NEJMoa1703784.

Buccino, A.P., Hurwitz, C.L., Garcia, S., Magland, J., Siegle, J.H., Hurwitz, R., Hennig, M.H., 2020. SpikeInterface, a unified framework for spike sorting. eLife 9, e61834. doi:10.7554/eLife.61834.

Budke, M., Avecillas-Chasin, J.M., Villarejo, F., 2018. Implantation of depth electrodes in children using VarioGuide® frameless navigation system: technical note. Oper. Neurosurg. Hagerstown Md 15, 302–309. doi:10.1093/ons/opx192.

Buzsáki, G., Anastassiou, C.A., Koch, C., 2012. The origin of extracellular fields and currents — EEG, ECoG, LFP and spikes. Nat. Rev. Neurosci. 13, 407–420. doi:10.1038/nrn3241.

Chari, A., Thornton, R.C., Tisdall, M.M., Scott, R.C., 2020. Microelectrode recordings in human epilepsy: a case for clinical translation. Brain Commun. 2, fcaa082. doi:10.1093/braincomms/fcaa082.

Chaure, F.J., Rey, H.G., Quian Quiroga, R., 2018. A novel and fully automatic spike-sorting implementation with variable number of features. J. Neurophysiol. 120, 1859–1871. doi:10.1152/jn.00339.2018.

Crandall, P.H., Walter, R.D., Rand, R.W., 1963. Clinical applications of studies on stereotactically implanted electrodes in temporal-lobe epilepsy. J. Neurosurg. 20, 827–840. doi:10.3171/jns.1963.20.10.0827.

Despouy, E., Curot, J., Denuelle, M., Deudon, M., Jean-Christophe-Sol Lotterie, J.-A., Reddy, L., Nowak, L.G., Pariente, J., Thorpe, S.J., Valton, L., Barbeau, E.J., 2019. Neuronal spiking activity highlights a gradient of epileptogenicity in human tuberous sclerosis lesions. Clin. Neurophysiol. doi:10.1016/j.clinph.2018.12.013.

Despouy, E., Curot, J., Reddy, L., Nowak, L.G., Deudon, M., Sol, J.-C., Lotterie, J.-A., Denuelle, M., Maziz, A., Bergaud, C., Thorpe, S.J., Valton, L., Barbeau, E.J., 2020. Recording local field potential and neuronal activity with tetrodes in epileptic patients. J. Neurosci. Methods 341, 108759. doi:10.1016/j.jneumeth.2020.108759.

Ducorps, A., Lemarechal, J.-D., Schwartz, D., Yahia-Cherif, L., 2010. A user-friendly software suite for MEG, EEG, EcoG /Intracranial-EEG data analysis. Presented at the Biomag - 17th International Conference on Biomagnetism, Dubrovnik, Croatia.

Ekstrom, A.D., Kahana, M.J., Caplan, J.B., Fields, T.A., Isham, E.A., Newman, E.L., Fried, I., 2003. Cellular networks underlying human spatial navigation. Nature 425, 184–188. doi:10.1038/nature01964.

Elahian, B., Lado, N.E., Mankin, E., Vangala, S., Misra, A., Moxon, K., Fried, I., Sharan, A., Yeasin, M., Staba, R., Bragin, A., Avoli, M., Sperling, M.R., Engel, J., Weiss, S.A., 2018. Low-voltage fast seizures in humans begin with increased interneuron firing: excitatory/inhibitory imbalance and LVF onset seizures. Ann. Neurol. doi:10.1002/ana.25325.

Engel, A.K., Moll, C.K.E., Fried, I., Ojemann, G.A., 2005. Invasive recordings from the human brain: clinical insights and beyond. Nat. Rev. Neurosci. 6, 35–47. doi:10.1038/nrn1585.

Fedorov, A., Beichel, R., Kalpathy-Cramer, J., Finet, J., Fillion-Robin, J.-C., Pujol, S., Bauer, C., Jennings, D., Fennessy, F., Sonka, M., Buatti, J., Aylward, S., Miller, J.V., Pieper, S., Kikinis, R., 2012. 3D Slicer as an image computing platform for the quantitative imaging network. Magn. Reson. Imaging 30, 1323–1341. doi:10.1016/j.mri.2012.05.001.

Fernandez-Vidal, S., Frazzini, V., Lambrecq, V., Navarro, V., Dormont, D., Mathon, B., Adam, C., Bardinet, E., Hasboun, D., 2019. Modular Stereotactic Planning Toolbox for SEEG Procedures Presented at the World Society for Stereotactic and Functional Neurosurgery.

Fisher, R.S., Webber, W.R., Lesser, R.P., Arroyo, S., Uematsu, S., 1992. High-frequency EEG activity at the start of seizures. J. Clin. Neurophysiol. Off. Publ. Am. Electroencephalogr. Soc. 9, 441–448. doi:10.1097/00004691-199207010-00012.

Fried, I., MacDonald, K.A., Wilson, C.L., 1997. Single neuron activity in human hippocampus and amygdala during recognition of faces and objects. Neuron 18, 753–765. doi:10.1016/s0896-6273(00)80315-3.

Holdgraf, C., Appelhoff, S., Bickel, S., Bouchard, K., D’Ambrosio, S., David, O., Devinsky, O., Dichter, B., Flinker, A., Foster, B.L., Gorgolewski, K.J., Groen, I., Groppe, D., Gunduz, A., Hamilton, L., Honey, C.J., Jas, M., Knight, R., Lachaux, J.-P., Lau, J.C., Lee-Messer, C., Lundstrom, B.N., Miller, K.J., Ojemann, J.G., Oostenveld, R., Petridou, N., Piantoni, G., Pigorini, A., Pouratian, N., Ramsey, N.F., Stolk, A., Swann, N.C., Tadel, F., Voytek, B., Wandell, B.A., Winawer, J., Whitaker, K., Zehl, L., Hermes, D., 2019. iEEG-BIDS, extending the brain imaging data structure specification to human intracranial electrophysiology. Sci. Data 6, 102. doi:10.1038/s41597-019-0105-7.

Howard, M.A., Volkov, I.O., Granner, M.A., Damasio, H.M., Ollendieck, M.C., Bakken, H.E., 1996. A hybrid clinical-research depth electrode for acute and chronic in vivo microelectrode recording of human brain neurons. Technical note. J. Neurosurg. 84, 129–132. doi:10.3171/jns.1996.84.1.0129.

Jurczynski, P., Cam, S., Rossion, B., Ranta, R., 2021. Separating local and propagated contributors to the Behnke-fried microelectrode recordings. In: Proceedings of the 14th International Joint Conference on Biomedical Engineering Systems and Technologies. Presented at the 14th International Conference on Bio-inspired Systems and Signal Processing. SCITEPRESS - Science and Technology Publications, pp. 343–350 Online Streaming, — Select a Country — doi:10.5220/0010349303430350.

Keller, C.J., Truccolo, W., Gale, J.T., Eskandar, E., Thesen, T., Carlson, C., Devinsky, O., Kuzniecky, R., Doyle, W.K., Madsen, J.R., Schomer, D.L., Mehta, A.D., Brown, E.N., Hochberg, L.R., Ulbert, I., Halgren, E., Cash, S.S., 2010. Heterogeneous neuronal firing patterns during interictal epileptiform discharges in the human cortex. Brain 133, 1668–1681. doi:10.1093/brain/awq112.

Khodagholy, D., Gelinas, J.N., Thesen, T., Doyle, W., Devinsky, O., Malliaras, G.G., Buzsáki, G., 2015. NeuroGrid: recording action potentials from the surface of the brain. Nat. Neurosci. 18, 310–315. doi:10.1038/nn.3905.

Kim, K., Ladenbauer, J., Babo-Rebelo, M., Buot, A., Lehongre, K., Adam, C., Hasboun, D., Lambrecq, V., Navarro, V., Ostojic, S., Tallon-Baudry, C., 2019. Resting-state neural firing rate is linked to cardiac-cycle duration in the human cingulate and parahippocampal cortices. J. Neurosci. Off. J. Soc. Neurosci. 39, 3676–3686. doi:10.1523/JNEUROSCI.2291-18.2019.

Kornblith, S., Quian Quiroga, R., Koch, C., Fried, I., Mormann, F., 2017. Persistent single-neuron activity during working memory in the human medial temporal lobe. Curr. Biol. CB 27, 1026–1032. doi:10.1016/j.cub.2017.02.013.

Kreiman, G., Koch, C., Fried, I., 2000. Imagery neurons in the human brain. Nature 408, 357–361. doi:10.1038/35042575.

Lakretz, Y., Ossmy, O., Friedmann, N., Mukamel, R., Fried, I., 2021. Single-cell activity in human STG during perception of phonemes is organized according to manner of articulation. NeuroImage 226, 117499. doi:10.1016/j.neuroimage.2020.117499.

Lambrecq, V., Lehongre, K., Adam, C., Frazzini, V., Mathon, B., Clemenceau, S., Hasboun, D., Charpier, S., Baulac, M., Navarro, V., Le Van Quyen, M., 2017. Single-unit activities during the transition to seizures in deep mesial structures: seizures and single-unit activities. Ann. Neurol. 82, 1022–1028. doi:10.1002/ana.25111.

Mathon, B., Clemenceau, S., Hasboun, D., Habert, M.-O., Belaid, H., Nguyen-Michel, V.-H., Lambrecq, V., Navarro, V., Dupont, S., Baulac, M., Cornu, P., Adam, C., 2015. Safety profile of intracranial electrode implantation for video-EEG recordings in drug-resistant focal epilepsy. J. Neurol. 262, 2699–2712. doi:10.1007/s00415-015-7901-6.

Minxha, J., Mamelak, A.N., Rutishauser, U., 2018. Surgical and electrophysiological techniques for single-neuron recordings in human epilepsy patients. In: Sillitoe, R.V. (Ed.), Extracellular Recording Approaches, Neuromethods. Springer New York, New York, NY, pp. 267–293. doi:10.1007/978-1-4939-7549-5_14.

Misra, A., Burke, J., Ramayya, A., Jacobs, J., Sperling, M., Moxon, K., Kahana, M., Evans, J., Sharan, A., 2014. Methods for implantation of micro-wire bundles and optimization of single/multiunit recordings from human mesial temporal lobe. J. Neural Eng. 11, 026013. doi:10.1088/1741-2560/11/2/026013.

Mormann, F., Kornblith, S., Quiroga, R.Q., Kraskov, A., Cerf, M., Fried, I., Koch, C., 2008. Latency and selectivity of single neurons indicate hierarchical processing in the human medial temporal lobe. J. Neurosci. Off. J. Soc. Neurosci. 28, 8865–8872. doi:10.1523/JNEUROSCI.1640-08.2008.

Niediek, J., Boström, J., Elger, C.E., Mormann, F., 2016. Reliable analysis of single-unit recordings from the human brain under noisy conditions: tracking neurons over hours. PLoS One 11, e0166598. doi:10.1371/journal.pone.0166598.

Oostenveld, R., Fries, P., Maris, E., Schoffelen, J.-M., 2011. FieldTrip: open source software for advanced analysis of MEG, EEG, and invasive electrophysiological data. Comput. Intell. Neurosci. 2011, 156869. doi:10.1155/2011/156869.

Parvizi, J., Kastner, S., 2018. Promises and limitations of human intracranial electroencephalography. Nat. Neurosci. 21, 474–483. doi:10.1038/s41593-018-0108-2.

Paulk, A.C., Yang, J.C., Cleary, D.R., Soper, D.J., Halgren, M., O'Donnell, A.R., Lee, S.H., Ganji, M., Ro, Y.G., Oh, H., Hossain, L., Lee, J., Tchoe, Y., Rogers, N., Kiliç, K., Ryu, S.B., Lee, S.W., Hermiz, J., Gilja, V., Ulbert, I., Fabó, D., Thesen, T., Doyle, W.K., Devinsky, O., Madsen, J.R., Schomer, D.L., Eskandar, E.N., Lee, J.W., Maus, D., Devor, A., Fried, S.I., Jones, P.S., Nahed, B.V., Ben-Haim, S., Bick, S.K., Richardson, R.M., Raslan, A.M., Siler, D.A., Cahill, D.P., Williams, Z.M., Cosgrove, G.R., Dayeh, S.A., Cash, S.S., 2021. Microscale physiological events on the human cortical surface. Cereb. Cortex 31, 3678–3700. doi:10.1093/cercor/bhab040.

Pedreira, C., Martinez, J., Ison, M.J., Quian Quiroga, R., 2012. How many neurons can we see with current spike sorting algorithms? J. Neurosci. Methods 211, 58–65. doi:10.1016/j.jneumeth.2012.07.010.

Polikov, V.S., Tresco, P.A., Reichert, W.M., 2005. Response of brain tissue to chronically implanted neural electrodes. J. Neurosci. Methods 148, 1–18. doi:10.1016/j.jneumeth.2005.08.015.

Quiroga, R.Q., Reddy, L., Kreiman, G., Koch, C., Fried, I., 2005. Invariant visual representation by single neurons in the human brain. Nature 435, 1102–1107. doi:10.1038/nature03687.

Reif, P.S., Strzelczyk, A., Rosenow, F., 2016. The history of invasive EEG evaluation in epilepsy patients. Seizure 41, 191–195. doi:10.1016/j.seizure.2016.04.006.

Rey, H.G., Pedreira, C., Quian Quiroga, R., 2015. Past, present and future of spike sorting techniques. Brain Res. Bull., Adv. Electrophysiol. Data Anal. 119, 106–117. doi:10.1016/j.brainresbull.2015.04.007.

Ringel, F., Ingerl, D., Ott, S., Meyer, B., 2009. VarioGuide: a new frameless image-guided stereotactic system–accuracy study and clinical assessment. Neurosurgery 64, 365–371. doi:10.1227/01.NEU.0000341532.15867.1C, discussion 371-373.

Rivière, D., Geffroy, D., Denghien, I., Souedet, N., Cointepas, Y., 2011. Anatomist: a Python Framework for Interactive 3D Visualization of Neuroimaging Data Presented at the Python in Neuroscience Workshop.

Rutishauser, U., Reddy, L., Mormann, F., Sarnthein, J., 2021. The architecture of human memory: insights from human single-neuron recordings. J. Neurosci. Off. J. Soc. Neurosci. 41, 883–890. doi:10.1523/JNEUROSCI.1648-20.2020.

Schevon, C.A., Ng, S.K., Cappell, J., Goodman, R.R., McKhann, G., Waziri, A., Branner, A., Sosunov, A., Schroeder, C.E., Emerson, R.G., 2008. Microphysiology of epileptiform activity in human neocortex. J. Clin. Neurophysiol. 25, 321–330. doi:10.1097/WNP.0b013e31818e8010.

Schevon, C.A., Weiss, S.A., McKhann, G., Goodman, R.R., Yuste, R., Emerson, R.G., Trevelyan, A.J., 2012. Evidence of an inhibitory restraint of seizure activity in humans. Nat. Commun. 3, 1060. doi:10.1038/ncomms2056.

Soleil, D., Badier, J.-M., Lemesle, M., 1992. Zero" solution for shielding and electrical protection in a unit for electroencephalographic recording. In: 1992 14th Annual International Conference of the IEEE Engineering in Medicine and Biology Society. Presented at the 1992 14th Annual International Conference of the IEEE Engineering in Medicine and Biology Society, pp. 1134–1135. doi:10.1109/IEMBS.1992.5761389.

Staba, R.J., Stead, M., Worrell, G.A., 2014. Electrophysiological biomarkers of epilepsy. Neurother. J. Am. Soc. Exp. Neurother. 11, 334–346. doi:10.1007/s13311-014-0259-0.

Stacey, W.C., Kellis, S., Greger, B., Butson, C.R., Patel, P.R., Assaf, T., Mihaylova, T., Glynn, S., 2013. Potential for unreliable interpretation of EEG recorded with microelectrodes. Epilepsia 54, 1391–1401. doi:10.1111/epi.12202.

Staresina, B.P., Reber, T.P., Niediek, J., Boström, J., Elger, C.E., Mormann, F., 2019. Recollection in the human hippocampal-entorhinal cell circuitry. Nat. Commun. 10, 1503. doi:10.1038/s41467-019-09558-3.

Stead, M., Bower, M., Brinkmann, B.H., Lee, K., Marsh, W.R., Meyer, F.B., Litt, B., Van Gompel, J., Worrell, G.A., 2010. Microseizures and the spatiotemporal scales of human partial epilepsy. Brain J. Neurol. 133, 2789–2797. doi:10.1093/brain/awq190.

Talairach, J., Bancaud, J., 1966. Lesion, "irritative" zone and epileptogenic focus. Confin. Neurol. 27, 91–94. doi:10.1159/000103937.

Truccolo, W., Donoghue, J.A., Hochberg, L.R., Eskandar, E.N., Madsen, J.R., Anderson, W.S., Brown, E.N., Halgren, E., Cash, S.S., 2011. Single-neuron dynamics in human focal epilepsy. Nat. Neurosci. 14, 635–641. doi:10.1038/nn.2782.

Ulbert, I., Heit, G., Madsen, J., Karmos, G., Halgren, E., 2004. Laminar analysis of human neocortical interictal spike generation and propagation: current source density and multiunit analysis in vivo. Epilepsia 45, 48–56. doi:10.1111/j.0013-9580.2004.04011.x.

Verzeano, M., Crandall, P.H., Dymond, A., 1971. Neuronal activity of the amygdala in patients with psychomotor epilepsy. Neuropsychologia 9, 331–344. doi:10.1016/0028-3932(71)90029-7.

Weiss, S.A., Alvarado-Rojas, C., Bragin, A., Behnke, E., Fields, T., Fried, I., Engel, J., Staba, R., 2016. Ictal onset patterns of local field potentials, high frequency oscillations, and unit activity in human mesial temporal lobe epilepsy. Epilepsia 57, 111–121. doi:10.1111/epi.13251.

Wendling, F., Bartolomei, F., Bellanger, J.J., Bourien, J., Chauvel, P., 2003. Epileptic fast intracerebral EEG activity: evidence for spatial decorrelation at seizure onset. Brain J. Neurol. 126, 1449–1459. doi:10.1093/brain/awg144.

Wild, J., Prekopcsak, Z., Sieger, T., Novak, D., Jech, R., 2012. Performance comparison of extracellular spike sorting algorithms for single-channel recordings. J. Neurosci. Methods 203, 369–376. doi:10.1016/j.jneumeth.2011.10.013.

Wyler, A.R., Ojemann, G.A., Ward, A.A., 1982. Neurons in human epileptic cortex: correlation between unit and EEG activity. Ann. Neurol. 11, 301–308. doi:10.1002/ana.410110311.

Yger, P., Spampinato, G.L., Esposito, E., Lefebvre, B., Deny, S., Gardella, C., Stimberg, M., Jetter, F., Zeck, G., Picaud, S., Duebel, J., Marre, O., 2018. A spike sorting toolbox for up to thousands of electrodes validated with ground truth recordings in vitro and in vivo. eLife 7, e34518. doi:10.7554/eLife.34518.

Zijlmans, M., Worrell, G.A., Dümpelmann, M., Stieglitz, T., Barborica, A., Heers, M., Ikeda, A., Usui, N., Le Van Quyen, M., 2017. How to record high-frequency oscillations in epilepsy: a practical guideline. Epilepsia 58, 1305–1315. doi:10.1111/epi.13814.

Zijlmans, M., Zweiphenning, W., van Klink, N., 2019. Changing concepts in presurgical assessment for epilepsy surgery. Nat. Rev. Neurol. 15, 594–606. doi:10.1038/s41582-019-0224-y.